JOURNAL OF THE MECHANICAL BEHAVIOR OF BIOMEDICAL MATERIALS ▮ (▮▮▮▮) ▮▮▮–▮▮▮

Available online at www.sciencedirect.com

ScienceDirect

www.elsevier.com/locate/jmbbm

Review Paper

The materials science of collagen

Vincent R. Sherman[1,a,*], *Wen Yang*[b], *Marc A. Meyers*[a]

[a]*University of California, San Diego, United States*
[b]*ETH, Zürich, Switzerland*

ARTICLE INFO

Article history:
Received 17 October 2014
Received in revised form
23 May 2015
Accepted 25 May 2015

ABSTRACT

Collagen is the principal biopolymer in the extracellular matrix of both vertebrates and invertebrates. It is produced in specialized cells (fibroblasts) and extracted into the body by a series of intra and extracellular steps. It is prevalent in connective tissues, and the arrangement of collagen determines the mechanical response. In biomineralized materials, its fraction and spatial distribution provide the necessary toughness and anisotropy. We review the structure of collagen, with emphasis on its hierarchical arrangement, and present constitutive equations that describe its mechanical response, classified into three groups: hyperelastic macroscopic models based on strain energy in which strain energy functions are developed; macroscopic mathematical fits with a nonlinear constitutive response; structurally and physically based models where a constitutive equation of a linear elastic material is modified by geometric characteristics. Viscoelasticity is incorporated into the existing constitutive models and the effect of hydration is discussed. We illustrate the importance of collagen with descriptions of its organization and properties in skin, fish scales, and bone, focusing on the findings of our group.

Contents

*Corresponding author. Tel.: +1 530 308 3842.
E-mail address: vsherman@ucsd.edu (V.R. Sherman).
[1]Mailing address: Mechanical and Aerospace Engineering, Mail Stop 411, 9500 Gilman Dr., La Jolla, CA 92037, United States.

http://dx.doi.org/10.1016/j.jmbbm.2015.05.023
1751-6161/

Please cite this article as: Sherman, V.R., et al., The materials science of collagen. Journal of the Mechanical Behavior of Biomedical Materials (2015), http://dx.doi.org/10.1016/j.jmbbm.2015.05.023

1. Types of collagen and its ubiquity in nature

Collagen is a structural biological polymer of upmost importance. Over 200,000 articles have been written about collagen, divulging the intricacies of this biopolymer which is the key ingredient of connective tissues. It is prevalent in tendons, skin, blood vessels, cornea, and coordinates with minerals to make bones, teeth, fish scales, and cartilage. Collagen makes up to 30% of the mass of vertebrates and lays their structural framework. Due to its ubiquity and importance, collagen has been nicknamed the “steel of biological materials”.

Collagen comes in many forms throughout nature. Each polypeptide molecule is a left-handed chain (Fig. 1a); three polypeptide molecules form a right handed triple helical structure (Fig. 1b). Each helical structure is called tropocollagen (Gelse et al., 2003). Each polypeptide chain (also called procollagen) contains a region characterized by a repeating amino acid motif: Gly-X-Y where Gly is a glycine and X or Y can be any amino acid. Glycine is at the core of the protein, while the X and Y amino acids are exposed at the surface.

The triple helical region is a major part of most collagens, but in some cases it can be only a minor part with other large non-collagenous domains of the molecule. In humans, there are 28 proteins known as collagens, as well as many other proteins which are considered part of the collagen superfamily. Collagens are classified into several general groups: fibrillar collagens, FACIT (Fibril Associated Collagens with Interrupted Triple Helices) and FACIT-like collagens, beaded filament collagens, basement membrane collagens, short chain collagens, transmembrane collagens, as well as some unclassified collagens. The most common form of collagen is type I, which is a fibrillar collagen (Hulmes, 2008). However, a brief description of the various classes is presented below.

1.1. *Fibrillar collagens*

Fibrillar collagens are characterized by a characteristic *d*-banding pattern, where a staggered collagen arrangement creates visible bands on the fibrils produced. Highly organized fibrils and fibers provide structural support throughout the body including in bones, skin, tendons, cartilage, dentin, blood vessels, nerves, intestines, and in the fibrous capsules of organs.

The structural hierarchy is illustrated in Fig. 1c. Hydrated collagen molecules of ~1.6 nm (Smith, 1968) diameter and ~299 nm length (as packed within fibrils) are staggered by integral multiples of ~67 nm, or one *d*-period (Orgel et al., 2011). The two-dimensional version of this is shown, but in three dimensions it becomes impossible to maintain equal staggering with all adjacent molecules (Smith, 1965). In order to maximize the number of quarter staggered molecules, Smith (1968) proposed a collagen filament composed of five molecules in cross-section where each molecule is staggered by one *d*-period. These five-molecule arrangements, called microfibrils, correspond to the observation of 2–3 nm diameter collagenous structures and is the only reasonable geometric arrangement to reflect these observations (Smith, 1968; Olsen, 1963). Each molecule is 4.46 *d* long, and a gap of 0.54 *d* (~36 nm) lies at the ends of non-overlapping molecules. There is also an overlap of 0.46 *d*, or 31 nm between adjacent molecules. The 0.54 *d* length empty period along with the 0.46 *d* overlap lead to the full 67 nm *d*-period. This overlapping pattern is called the quarter-staggered assembly (Vuorio and Decrombrugghe, 1990).

A full crystallographic description of type I fibrillar collagen supermolecular structure was presented by Orgel et al. (2006) and is shown in Fig. 2. The electron density map of Fig. 2a shows the collagen molecules forming a helicoid around the axis; the microfibril has a supermolecular right-

Please cite this article as: Sherman, V.R., et al., The materials science of collagen. Journal of the Mechanical Behavior of Biomedical Materials (2015), http://dx.doi.org/10.1016/j.jmbbm.2015.05.023

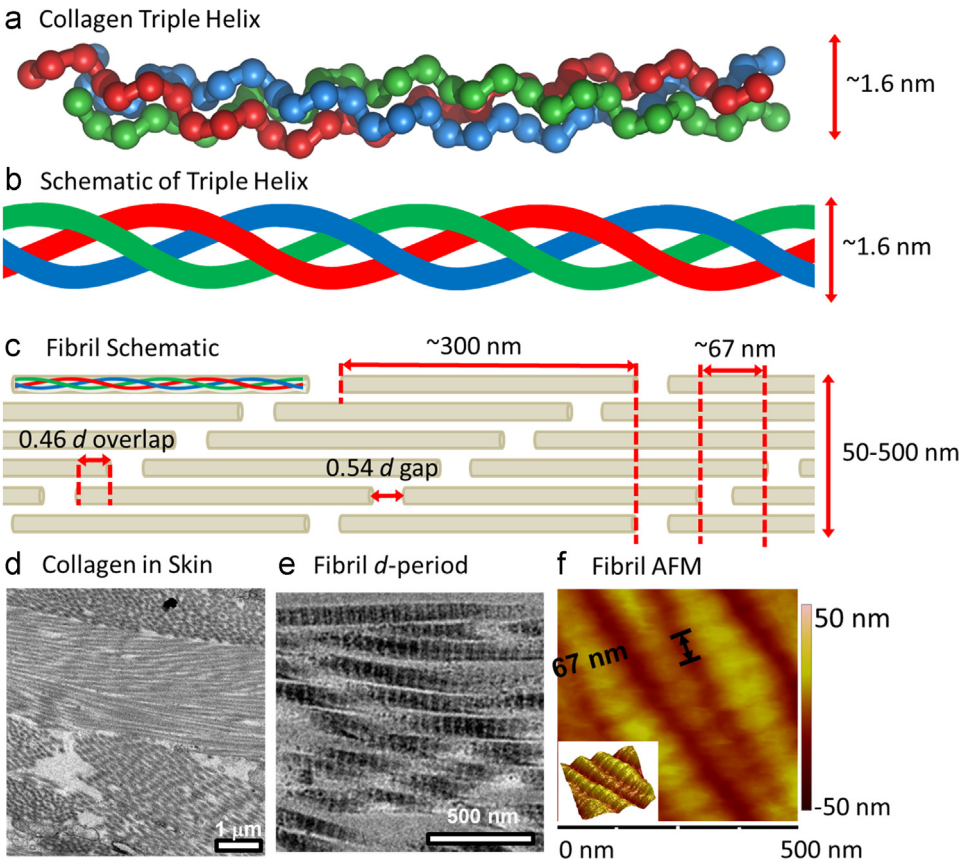

Fig. 1 – Structural hierarchy of fibrillar collagen. (a) In collagen formations, helical left-handed procollagen chains (Red, Green, Blue) form a right-handed triple helix of roughly 300 nm in length. (b) Schematic representation of triple helix formed by three procollagen chains. (c) Arrangement of triple helices into fibrils. Triple helices are arranged in a staggered manner, leading to a gap (0.54 *d*) and an overlap (0.46 *d*) region. The gap region has less triple helices across the section, and the overlap region has more. This gap and overlap has a periodicity, or *d*-period, of ~67 nm, and is the cause of the visible banding in collagen fibrils. (d) Layers of collagen fibrils in a cross-section of skin. (e) Collagen fibrils of 100 nm diameter imaged by TEM. Fibrils clearly display the characteristic banding feature. Due to the viewing angle of the fibrils, *d*-period measurements decrease proportionally to the cosine of the viewing angle. A 90 degree viewing angle would lead to perfectly accurate measurements. (f) AFM by Yang et al. (2014) of hydrated collagen fibrils in an arapaima scale. 67 nm *d*-period is measured. (For interpretation of the references to color in this figure legend, the reader is referred to the web version of this article.)

handed twist. This is also shown in Fig. 2c. Thus, there are three helices: polypeptide chains (left handed), collagen chains (right handed), and microfibrils (right handed) consisting of five collagen chains. The molecules have a quasi-hexagonal packing pattern, and the maps confirm that each microfibril consists of five molecules in the overlap region. This detailed description of the packing of molecular collagen is a powerful tool for the understanding and modeling of the collagen fibril.

1.2. FACIT collagens

Fibril associated collagens with interrupted triple helices are abbreviated FACIT collagens. FACIT collagens are thus named due to their associations and interactions with collagen fibrils. They have collagenous domains which are interrupted by non-helical domains, and associate with the surface of collagen fibrils. Type IX collagen, for example, is a FACIT collagen which lies anti-parallel along type II fibrils (Wu et al., 1992). A hinge region provides flexibility between the collagen cross-linked with type II fibrils and a terminal domain which is available for interactions with matrix constituents (Vanderrest and Mayne, 1988). However, some FACITs are not actually known to interact with collagen fibrils; these collagens are classified based on the primary sequence which is similar to that of type IX, XII and XIV collagen, which have been shown to interact directly with fibrillar collagen molecules (Gelse et al., 2003; Bächinger et al., 2010; Myllyharju and Kivirikko, 2001).

1.3. Beaded filament collagen

There is only one beaded filament collagen, type VI. Type VI collagen is composed of beaded filaments with short triple helical regions, and is about one third the length of fibrillar collagens. Type VI collagen plays an important role in maintaining tissue integrity. The beaded filament collagens have large N and C terminal regions, and molecules assemble into filaments

Please cite this article as: Sherman, V.R., et al., The materials science of collagen. Journal of the Mechanical Behavior of Biomedical Materials (2015), http://dx.doi.org/10.1016/j.jmbbm.2015.05.023

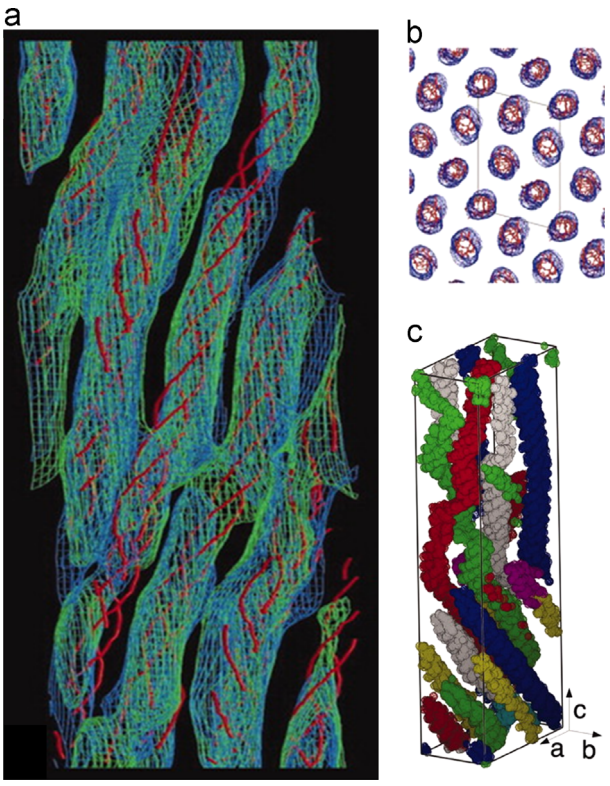

Fig. 2 – Collagen structure as presented by Orgel et al. (2006). (a) Electron density map of a collagen microfibril consisting of five collagen molecule segments, and showing the right-handed supermolecular twist. (b) Unit cell marked around fibril crossections, showing the quasihexagonal packing of the molecular segments. (c) Molecular path of a collagen molecule through multiple unit cells.

with a periodicity of 110 nm. However, the terminal regions are not cleaved during assembly. These uncleaved terminal regions cause a periodic bead region throughout the collagen filament (Bächinger et al., 2010).

1.4. *Basement membrane collagens*

The basement membrane is a matrix under the cavities of the epithelium lining and surfaces of organs including skin, and the endothelium in the interior of blood vessels. Basement membrane collagen (type IV) creates specialized structures found at tissue boundaries. It forms relatively thin sheets of 40–50 nm thick interlaced networks, which aid in molecular filtration. The network is a fine meshwork structure of many branches, about 20 nm between branching points (Hulmes, 2008; Bächinger et al., 2010; Kadler et al., 2007). Other collagens found in the basement membrane zone include collagen VII, which creates anchoring filaments of about two molecules in length, and collagens XVIII and XV, which are crucial to eye and muscular development, respectively.

1.5. *Short chain collagens*

Short chain collagens (VIII and X) are meshwork forming collagens. The triple helical region is short: about half the length of fibrillar collagen. Type VIII collagen forms a hexagonal meshwork of thin fibrils, and functions as an enhancer of growth factor induced proliferation of cells. Type X collagen localizes in the hypertrophic zone of mineralizing cartilage (Bächinger et al., 2010).

1.6. *Transmembrane collagens*

Transmembrane collagens span the plasma membrane of cells, binding to extracellular and sometimes intracellular ligands. They are subject to shedding in vivo and in vitro, and are multifunctional, serving as a matrix receptor when membrane-bound and a signaling factor when soluble (Franzke et al., 2005). Additionally, transmembrane collagens play an important role in adhesion (Hulmes, 2008). In this overview we focus on the most abundant type of collagen, fibrillar collagens.

2. Genesis and formation of fibrillar collagen: from inside the cell to the formation of fibers

Collagen biosynthesis is a complex and deeply explored process. While it was once believed that the organization of collagen was a "self-assembly" process, where secreted collagen molecules would be ejected into intercellular space and self-assemble, this idea is no longer fully accepted (Gelman et al., 1979; Leslie, 2006). What is clear is that the formation of collagen fibrils does not occur in one step, but requires intracellular and extracellular stages which lead to the production of the common fiber (Trelstad et al., 1976). Birk and Trelstad (1986) identified pockets in the membranes of collagen producing fibroblasts which suggested that the fibroblast coordinated collagen assembly. The fibril formation process in a simplified manner is outlined in Fig. 3, beginning with the synthesis of procollagen chains on ribosomes (Fig. 3a). These polypeptide procollagen chains are imported into the rough endoplasmic reticulum (ER) (Fig. 3b) where, after a series of posttranslational steps, three chains combine to make a triple helical procollagen molecule. Stabilization of this molecule is due largely to hydroxylation of proline and hydroxyproline which, combined, make up about 20% of the total amino acids in human fibrillar collagens; hydroxylation of these amino acids leads to hydrogen bonding and the electron withdrawing effect (Brodsky and Persikov, 2005).

Procollagen molecules transit via the Golgi complex (Fig. 3c) where they are packaged into secretory vesicles, called Golgi to plasma membrane carriers. During this packaging and transportation in the vesicles (Fig. 3d), C- terminal processing, or removal of the procollagen propeptides by proteinases begins. Although procollagen processing was believed to be a completely extracellular event, N- and C-proteinases have been identified in the Golgi network, and the C-proteinases have been shown to be active (Leighton and Kadler, 2003; Wang et al., 2003). Canty et al. (2004) showed that in embryonic tendon fibroblasts, some Golgi to plasma membrane carriers contain fibrils. Once formed, fibrils are subsequently stabilized by the formation of covalent crosslinks based on the reactions of aldehydes which are generated enzymatically from lysine or hydroxylysine side-chains (Eyre and Wu, 2005). Golgi to plasma membrane carriers then push out of the plasma membrane, creating a protrusion called a fibripositor (fibril depositor, Fig. 3e).

Please cite this article as: Sherman, V.R., et al., The materials science of collagen. Journal of the Mechanical Behavior of Biomedical Materials (2015), http://dx.doi.org/10.1016/j.jmbbm.2015.05.023

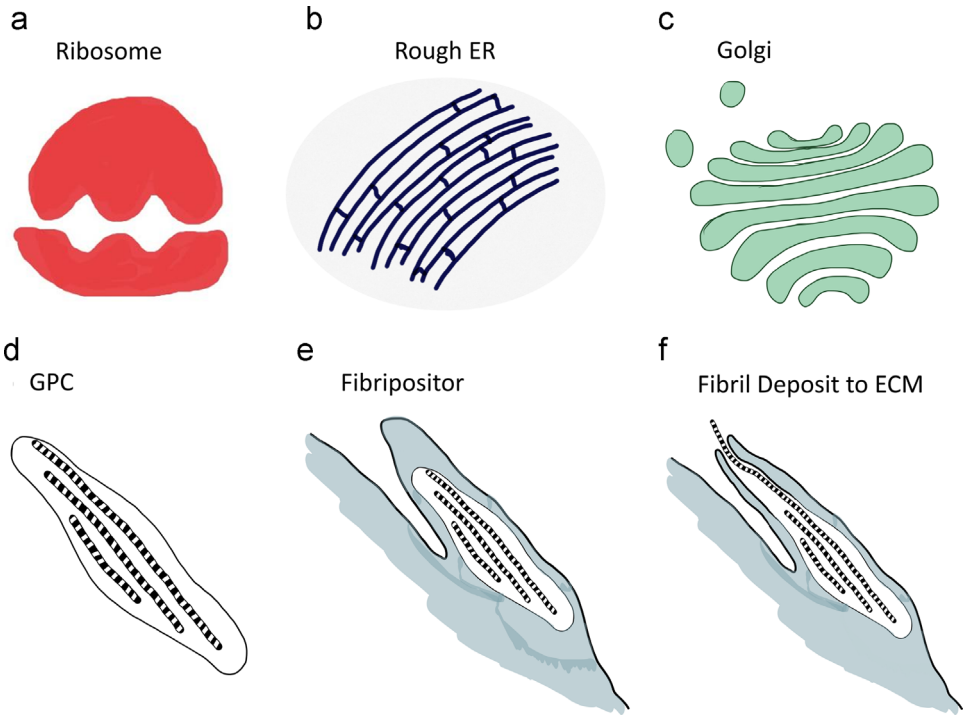

Fig. 3 – Formation of a collagen fibril. (a) The formation of a collagen fibril begins where the Ribosome synthesizes procollagen chains. (b) The ribosome imports new procollagen chains into the rough endoplasmic reticulum. Posttranslational modifications result in assembly of procollagen molecules. (c) The Golgi pack procollagen molecules into secretory vessels, called Golgi to plasma membrane carriers (GPCs). (d) GPC package after separating from Golgi apparatus. (e) A fibripositor (fibril depositor) is formed as the GCPs pushes out of the plasma membrane of the cell, preparing to deposit a fibril. (f) The fibripositor opens and deposits a fibril into the ECM.

Fibripositors have thus far been identified in tendon (Canty et al., 2004), fibrohistiocytic tumors (Pasquinelli, 2010), and corneal structures (Birk and Trelstad, 1986), and have become a common model used to explain the production of the fibril architecture in highly anisotropic, load bearing collagen arrays (Bhole et al., 2009). An alternative model suggests that fibrils condense from highly concentrated liquid crystalline solutions of tropocollagen monomer. Trelstad (1982) concluded that physical forces lead to the alignment of collagen structures, and Ruberti and Zieske (2008) have produced supporting evidence of this model by the creation of aligned collagen structures by simply confining monomer solutions between two featureless surfaces. Assembly from a liquid crystalline solution would simplify the collagen matrix assembly, and is consistent with some observations (Hay and Revel, 1969; Cintron et al., 1983).

Fibripositors proceed to fuse with the plasma membrane of the cell. Once fused with the cell surface, fibripositors create invaginations. Early fibrils project from these invaginations, and newly formed fibrils are delivered to the extracellular matrix (Fig. 3f), guided by adjacent fibroblasts, to their final structural configuration. At this point, the fibril framework has been laid (Canty et al., 2004). Further growth to fibril diameter and length is contributed by fusion of intermediates to the deposited highly ordered core. Intermediates include pN-collagen (N-propeptide), pC-collagen (C-propeptide), and fibril segments (Silver et al., 2003). Thus, the production of collagen involves a complex sequence of intra and extracellular steps.

3. Mechanical response of fibrillar collagen

The mechanical response of fibrillar collagen can be evaluated at different scales including: the molecular scale, the response of an individual molecule; the fibrillar scale, the response of the individual fibril; the microscale, the response of a collagen fiber; and the macroscale, the response of a collagenous tissue. Over time, many investigations have been performed at these different scales, and in some cases there are large variances in results across the same hierarchical level. Additional hierarchical levels have been described such as the microfibril, subfibril, and fascicle (Haut, 1986), but the majority of research regarding the mechanical response of collagen has focused on the following levels: molecule, fibril, fiber, and tissue. Table 1 compares the response of collagen at multiple hierarchical levels. One aspect which is significant is that the elastic modulus decreases as one marches up the hierarchical spatial scale. This is due to interfibrillar sliding at the lower scale and interfiber sliding at the larger scale as well as the straightening and reorientation of the fibrils/fibers.

Molecular dynamics simulations have become a key tool used to further the understanding of collagenous-based tissues. In order to effectively simulate collagen, it is crucial to have a good understanding of the molecular structure and packing arrangement of collagen molecules within the fibril. The earliest simulations were based on short, ~10 nm collagen-like peptides based on information from X-ray crystallography (Gautieri et al., 2011). Knowledge of the

Please cite this article as: Sherman, V.R., et al., The materials science of collagen. Journal of the Mechanical Behavior of Biomedical Materials (2015), http://dx.doi.org/10.1016/j.jmbbm.2015.05.023

Table 1 – Comparison of Young's modulus of collagen at multiple hierarchical levels.

Molecular	
Single molecule stretching, atomistic modeling (Lorenzo and Caffarena, 2005)	4.8 GPa
Single molecule stretching, reactive atomistic modeling (Buehler, 2006)	7 GPa
Single molecule stretching, atomistic modeling (Vesentini et al., 2005)	2.4 GPa
Coarse grain modeling (Gautieri et al., 2010)	4 GPa
Atomistic modeling (Gautieri et al., 2009)	4 GPa
Atomistic modeling (Pradhan et al., 2011)	4.5–6.2 GPa (long, short molecule)
X-ray diffraction (Sasaki and Odajima, 1996)	3 GPa
Brillouin light scattering (Harley et al., 1977)	9 GPa
Brillouin light scattering (Cusack and Miller, 1979)	5.1 GPa
Estimate from persistent length (Hofmann et al., 1984)	3 GPa
Estimate from persistent length (Nestler et al., 1983)	4.1 GPa
Estimate from persistent length (Sun et al., 2002)	0.35–12 GPa
Microfibril and Fibril	
MEMS stretching (Eppell et al., 2006)	0.4–0.5 GPa low strain, 12 GPa high strain
MEMS stretching (Shen et al., 2008)	0.86 GPa low strain
X-ray diffraction (Gupta et al., 2004)	1 GPa
X-ray diffraction (Sasaki and Odajima, 1996)	0.43 GPa
AFM testing (van der Rijt et al., 2006)	0.2–0.8 GPa aqueous, 2–7 GPa ambient,
Bead and string based mesoscale modeling (Buehler, 2006, 2008)	4.4 GPa low strain, 38 GPa high strain
Atomistic modeling (Gautieri et al., 2011)	0.3 GPa small strain, 1.2 GPa high strain
Fiber	
Crosslinked rat tail tendon (Gentleman et al., 2003)	1.10 GPa
Non-crosslinked rat tail tendon (Gentleman et al., 2003)	50–250 MPa
Extruded, crosslinked fiber (Gentleman et al., 2003)	260–560 MPa
Rat tail tendon (Haut 1986)	960–1570 MPa
Rat tail tendon (Kato et al., 1989)	480–540 MPa
Extruded, crosslinked fiber (Kato et al., 1989)	170–550 MPa
Rabbit patellar tendon (Miyazaki and Hayashi, 1999)	30–80 MPa
Tissue	
Skin (Yang et al., 2015)	0–50 MPa
Tendon (Rigby et al., 1959)	1 GPa
Cornea (Orssengo and Pye, 1999)	0.2–1.0 MPa
Mitral valve (Freed and Doehring, 2005)	0–50 MPa

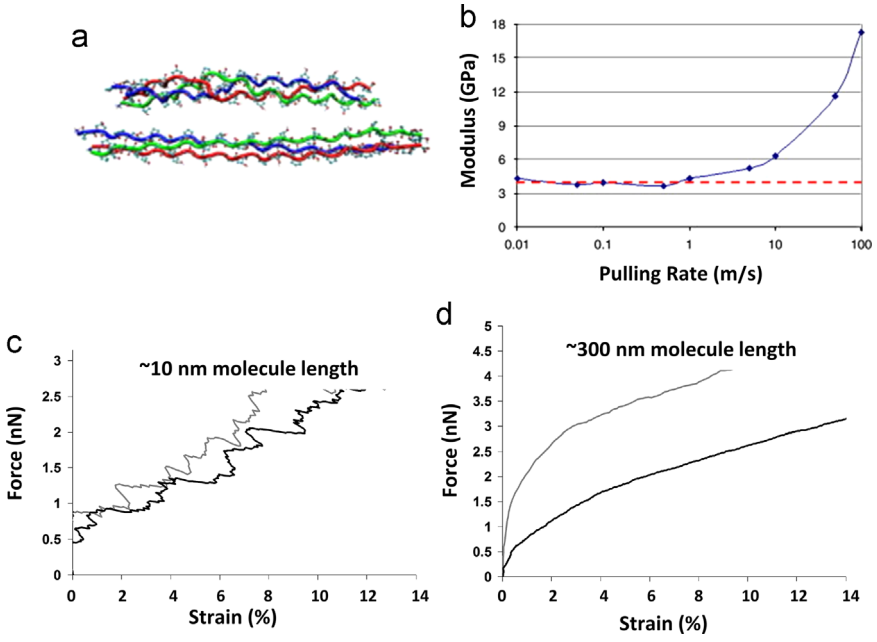

Fig. 4 – Mechanical response of molecular scale collagen. (a) A collagen triple helix subjected to extension. (b) Simulations by Gautieri et al. (2009) predict the mechanical response of the collagen triple helix. The modulus (increasing from 4 to 17 GPa) and its relationship to strain rate is illustrated. (c–d) Simulations of short and long molecules by Pradhan et al. (2011) show the importance of molecule length in the tensile response; short molecules lead to a sawtooth like force–displacement curve due to the breaking and recreation of hydrogen bonds.

collagen molecular structure has expanded, and now molecular packing data of type I collagen by Orgel et al. (2006) provide molecular resolution packing information. Combined with high resolution crystallography of collagen model peptides (Brodsky and Persikov, 2005; Okuyama et al., 2006), a whole molecule and tri-dimensional understanding of the structure of collagen is attained (Orgel et al., 2011).

3.1. *The molecular scale*

Multiple atomistic and coarse grain modeling simulations as well as a number of experimental methods have led to a variety of estimates of the molecular modulus of the collagen molecule. Fig. 4a shows a molecule being pulled in tension. Sasaki and Odajima (1996) used X-ray diffraction to measure the helical pitch of collagen molecules, and deduced the strain from the molecular pitch, this lead to an estimate of the modulus of 3.0 GPa. In separate studies, Cusack and Miller (1979) and Harley et al. (1977) used Brillouin light scattering to vibrate tendons, and extrapolated molecular moduli of 5.1 and 9 GPa, respectively. Atomistic modeling by Lorenzo and Caffarena (2005), Buehler (2006), Gautieri et al. (2009), and Vesentini et al. (2005), and coarse grain modeling by Gautieri et al. (2010) predicted moduli similar to experimental measurements, between 2.4 and 7 GPa (Gautieri et al., 2011). Fig. 4 highlights several important results of testing at the molecular scale; Fig. 4b presents the results of simulations by Gautieri et al. (2010) relating the elastic modulus at the molecular scale to the strain rate and showing that only above a certain rate there is a strong relationship between them. This critical rate helps determine an upper limit on strain rates during simulations in order to minimize computation time, which may be large due to the number of atoms in a collagen molecule (Gautieri et al., 2011). Pradhan et al. (2011) highlighted the importance that the length of the molecule plays, and simulated the modulus of short (8.5 nm) and long (300 nm) collagen molecules: 6.2 and 4.5 GPa. Fig. 4c and d shows that the short molecules have a saw-tooth like force–displacement curve due to the large proportion of hydrogen bonds being broken and reformed, while a longer molecule shows a much smoother curve; these results highlight the important considerations which must be accounted for when simulating the molecular response of collagen.

3.2. *The fibrillar scale*

The elastic modulus of collagen at the fibrillar scale is lower than the modulus at the molecular scale. Similar to tests of the individual molecule, the results of different fibril tests have produced a variety of results. Among wet fibrils, chosen due to their relevance to the in vivo condition, reported values of fibril modulus have a range from 0.2 GPa to 0.8 GPa at small strains. Testing methods used to measure fibrillar modulus include X-ray diffraction by Sasaki and Odajima (1996), where measured fibrillar strain is compared to tissue stress values (0.43 GPa), and AFM testing by van der Rijt et al. (2006), who pulled an individual hydrated fibril and recorded a modulus 0.2–0.8 GPa (increasing with strain). MEMS stretching of a single fibril by Eppell et al. (2006) and Shen et al. (2008) recorded moduli of 0.76 to 0.82 GPa. The experimental setup and results for nanoscale testing are shown in Fig. 5; AFM and MEMS testing is shown in Fig. 5a and b, and the AFM measured tensile response by van der Rijt et al. (2006) is shown in Fig. 5c. Atomistic and mesoscale modeling has been conducted by Buehler (2006, 2008) who estimated a range of 4.36–38 GPa, and more recently by Gautieri et al. (2011) who predicted 0.3–1.2 GPa, making note of the extreme importance of geometry, scale of observation, deformation state, and hydration level during simulations.

A degree of the variance in the results of mechanical testing can be understood based on Buehler's (2008) simulation of the effects of crosslink density on collagen fibrils. Crosslinks can be visualized as areas of increased adhesion between collagen molecules, seen in Fig. 6a. By varying the crosslink density from zero to approximately 3 per molecule, the stress which the fibril can support increases from less than 0.5 GPa to over 6 GPa. Additionally, the failure changes from a more gradual sliding to a brittle one as the density increases (Fig. 6b). The first regime is characterized by the breaking of hydrogen bonds and a lower modulus compared to the second region which becomes relevant at ~30% strain, and corresponds to the stretching of the molecular backbone of the collagen triple helix. It is only with sufficient molecular

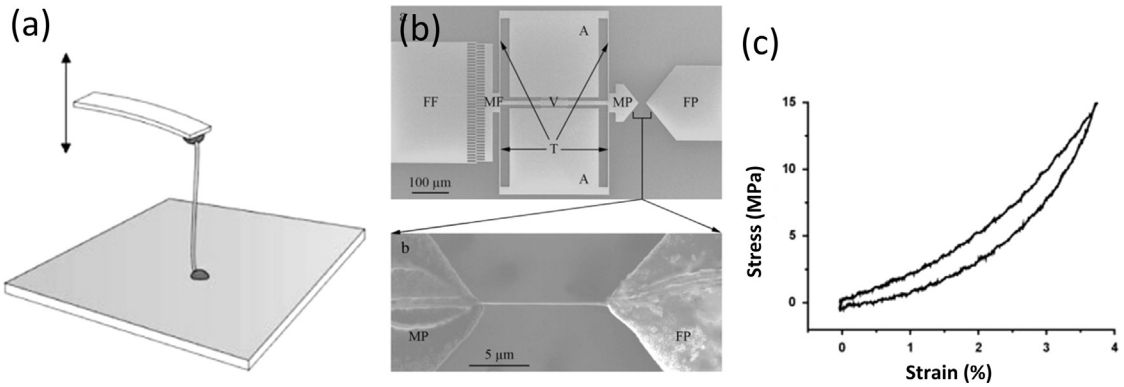

Fig. 5 – Mechanical response of collagen at fibrillar scale. Multiple tests have been done on collagen fibrils. (a) A test using AFM by van der Rijt et al. (2006), using glue to attach the fibril to the AFM tip and a base plate. (b) MEMS stretching of collagen fibril by Eppell et al. (2006). (c) Stress strain curve of wet collagen fibril by van der Rijt et al. (2006); dry measurements were also recorded, but the wet curve is shown because collagen fibrils are hydrated in the in vivo environment.

Please cite this article as: Sherman, V.R., et al., The materials science of collagen. Journal of the Mechanical Behavior of Biomedical Materials (2015), http://dx.doi.org/10.1016/j.jmbbm.2015.05.023

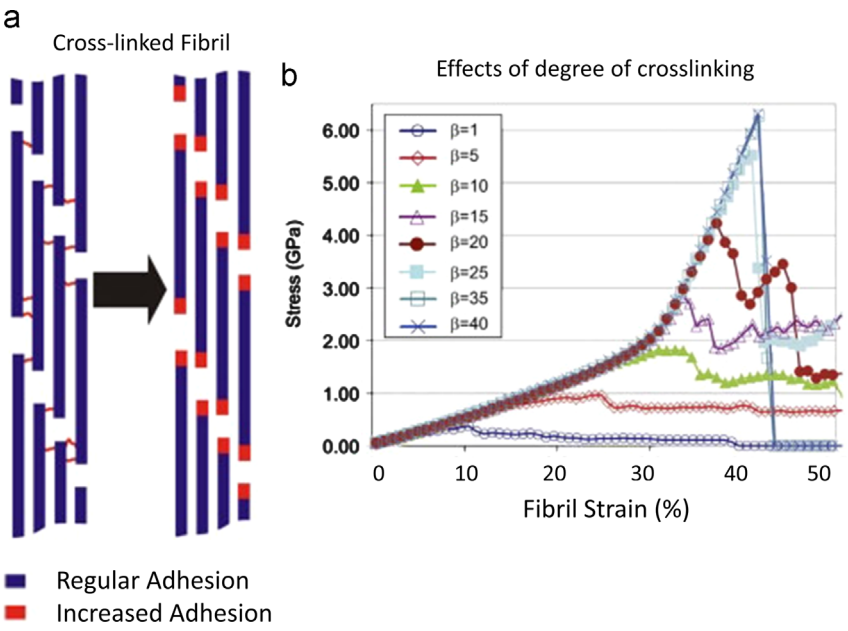

Fig. 6 – Crosslinking and mechanical response of fibrillar collagen. β is a parameter which is a linear representation of the degree of crosslinking; $\beta=15$ corresponds to one cross link per molecule, $\beta=30$ corresponds to two, etc. (a) Schematic showing schematic of cross-linked fibril with an average of one cross-link per molecule (corresponding to $\beta=15$.) (b) Simulations showing the effects of degree of crosslinking on a collagen fibril. At higher crosslink densities, there is a higher degree of adhesion between molecules; this leads to sufficient adhesion to enter the second elastic regime of increased modulus which corresponds to the stretching of the backbone of the collagen helix. The first elastic regime corresponds to breaking of hydrogen bonds between the helices of the collagen molecules. Schematic and simulation are results of Buehler (2008).

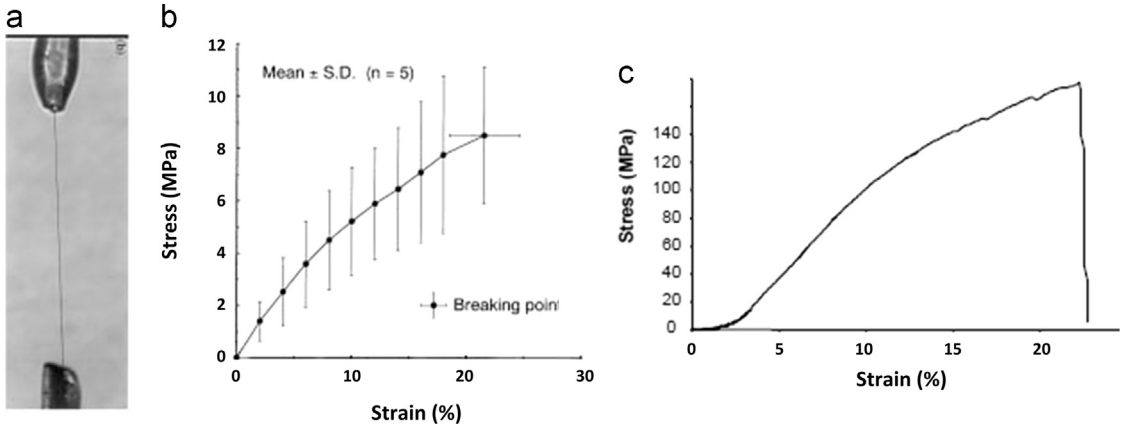

Fig. 7 – Mechanical response of collagen. (a) Microscale tests of a collagen fiber. (b) Stress strain relations from the rabbit patellar tendon by Miyazaki and Hayashi (1999). (c) Stress strain relations from the rat tail collagen fibers from Gentleman et al. (2003).

cross-linking that sliding can be averted, and this second regime is pertinent. One can conclude that the elastic modulus and fibrillar strength are dependent on the density of bonds between the molecules.

Molecular simulations are a crucial tool at the fibrillar level but computationally difficult because a single solvated collagen fibril contains billions of atoms (Gautieri et al., 2011). Even a single collagen molecule is computationally expensive due to the length of ~300 nm. In order to effectively model larger fibrils, atoms are assembled into large groups of up to 100 pseudo atoms; this is called coarse graining. The Martini model provides a more modest level of coarsening, where generally four atoms are grouped (Marrink et al., 2007).The resulting reduction in the number of particles also allows for a larger time step, and ultimately speeds up atomic simulations by 200–400 times (Vesentini et al., 2013). Over time, the modeled structure of collagen has improved, as available computational power has increased. Combined with advances in the methods of evaluating and incorporating the collagen molecular structure, the quality of simulations has continually improved. These advances continue to open many possibilities for future studies of collagen at the full fibril or even fiber level, and beyond. Section 6 shows how this method is applied to the elucidation of the mechanical response of the Bouligand-like structure of the Arapaima scale.

Please cite this article as: Sherman, V.R., et al., The materials science of collagen. Journal of the Mechanical Behavior of Biomedical Materials (2015), http://dx.doi.org/10.1016/j.jmbbm.2015.05.023

3.3. *The microscale*

Microscale tests are performed on the collagen fiber, which is a bundle of fibrils. A rather limited number of investigations have been performed at the microscale. Fibers have been extracted from rat tail tendon and tested by Gentleman et al. (2003) and Haut (1986). A tensile test of a collagen fiber is shown in Fig. 7a, and results are presented in Fig. 7b and c. Gentleman et al. (2003) concluded that modulus of fibers increases with strain rate (consistent with the MD predictions of Gautieri et al. (2009), shown in Fig. 4b), and increases with initial length, ranging from 50 to 250 MPa. It is also interesting to note that upon exposing these fibrils to a cross-linking agent, the modulus increases to ~1 GPa, on the order of the fibrillar strength. It is possible that by cross-linking the fiber and eliminating the interfibrillar sliding, the fibrillar stiffness may be realized at the fiber level. These tests were performed on rat tail fibers, which display properties changing with age and maturity. Throughout tissues, collagen fibers will inevitably display different properties due to natural differences such as shape, orientation, mineralization, and degree of cross-linking. Tendon is often chosen as an ideal material to study, because it is close to a pure and aligned collagen structure.

Collagen fibers are not present in all collagen-based structures. Structures which do include this hierarchical level include skin, tendon, and arteries. For example, the cornea does not have fibers, but rather fibrils which are organized in a highly ordered manner in order to allow transparency. Dentin consists of mineralized fibrils embedded in a mineral matrix. However, there are many instances where authors refer to collagen fibers in both the cornea and dentin, but this is due to discrepancies in the definition of fibrils and fibers. To further confuse the situation, a fibril may be described physically as a small fiber. But this should not confuse the fact that in the hierarchical structure of collagen, a fiber and fibril are unique levels which are not interchangeable and should not be confused. Other structures, such as the nails, hooves, and feathers do not have collagen at all.

3.4. *The macroscale*

At the macroscale, collagen fibrils and fibers may be arranged into a vast number of structures with extremely variable properties. Skin, tendon, and the cornea are all nearly exclusively collagen, yet specialized hierarchical organization generates properties which are vastly different.

Tendon has parallel and slightly wavy fibrils, with a very small low load extension of 2–3%, followed by a linear modulus and near failure a slightly decreased modulus. As strain increases, the crimp bands are extinguished (Fig. 8a). The modulus of tendon can be as high as 1 GPa (Rigby et al., 1959) and ultimate strength reaches 250 MPa (Yannas and Huang, 1972).

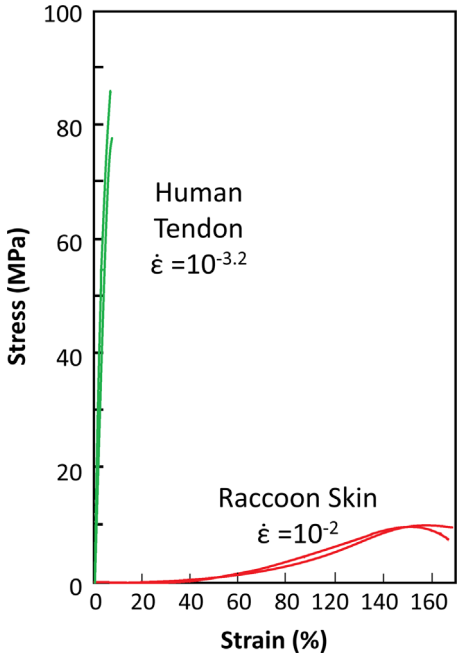

Fig. 9 – Illustration of the great variation in the mechanical response of collagen structures. A human tendon strains to less than 10% before rupture, at a stress of nearly 90 MPa (Benedict et al., 1968). Raccoon skin, in contrast, only supports ~10 MPa, but fails at a strain of nearly 150%. These vast differences of two collagen based structures show the extreme importance of the geometric organization of collagen fibrils.

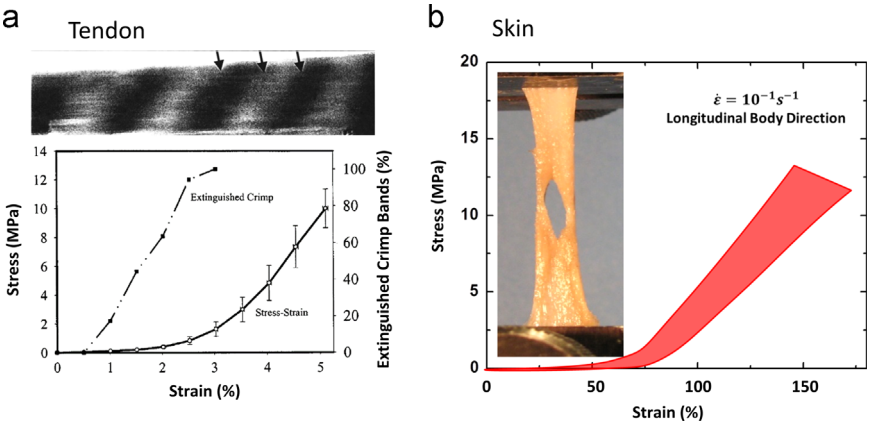

Fig. 8 – Mechanical response of collagen. (a) Macroscale tests of a tendon by Hansen et al. (2002). The visible crimp in the tendon is extinguished in the toe region of the curve, followed by a stiffening. (b) Macroscale tests of skin, showing a much larger toe region of the curve do to the extreme curvature of the collagen fibers.

Please cite this article as: Sherman, V.R., et al., The materials science of collagen. Journal of the Mechanical Behavior of Biomedical Materials (2015), http://dx.doi.org/10.1016/j.jmbbm.2015.05.023

Rabbit skin is made of a net of wavy collagen fibers, and may experience greater than 50% extension before sizeable load is carried, and a modulus which begins at zero, increasing with strain to ~50 MPa, and an ultimate strength of ~15 MPa. This unique response is shown in Fig. 8b. In order to visualize the extreme differences and range of mechanical behavior, the tensile responses of tendon and skin are shown in Fig. 9. The strength of tendon reaches values of ~90 MPa (Benedict et al., 1968), while skin has a typical strength of 10–20 MPa (raccoon skin shown, with a strength of 10 MPa). Accordingly, the maximum strain of skin is much higher (ε_{max}~0.5–1.5) than tendon (ε_{max}~0.1).

Another example is the cornea which is comprised of lamellae of highly ordered straight fibrils with identical size and spacing. This structure is optimized for transparency, but at a cost: a much lower strength than tendon at only ~20 MPa (Bryant et al., 1994). The vast differences in mesoscale properties of collagen-based tissues are due to the hierarchical organization and configuration of the molecules, fibrils, and fibers.

3.5. *Effects of mineralization*

Mineralized collagen structures are designed to carry compressive load, as mineral crystals minimize sliding and deformation of the collagen. Fig. 10a shows in a schematic manner the arrangement of minerals in bone. Mineral particles are deposited within (intrafibrillar) and on the surface (interfibrillar) of collagen fibrils, which leads to a fully mineralized composite matrix of protein and mineral components (Landis et al., 1996; Landis and Hodgens, 1996). Structures made of this composite, such as bone, dentin, and fish scales, all experience altered mechanical properties compared to non-mineralized tissues. Both the mineral and collagen form a continuous network. The most important differences are that the mineralized structures are much stiffer and much less extensible than non-mineralized structures in tension, and have a much higher compressive strength (Wainwright et al., 1982). This mineral is commonly referred to as hydroxyapatite, but in fact has a stoichiometrically deficient amount of hydroxyl (Rey et al., 1995; Cho et al., 2003). Carbonate ions substitute hydroxyl and make up a large portion of the stoichiometric deficiency (Pasteris et al., 2012). However, this is only one of a large number of possible substitutions, which include Na^{+} or Mg^{2+} replacing Ca^{2+} ions, HPO_4^{-2} replacing phosphate ions, Cl^{-1} and F^{-1} replacing OH^{-1}, and CO_3^{-2} replacing phosphate and hydroxyl (Fratzl et al., 2004). These substitutions are responsible for a lack of consistency in the literature as bone mineral may be referred to as apatite, hydroxyapatite, carbonated hydroxyapatite, and hydroxylapatite, among others. For the purpose of this review and to avoid confusion, the apatite-based component of bone will be referred to simply as mineral.

The result of the mineralization process is that collagen fibrils are impregnated with plate -shaped mineral particles which have dimensions of ~2 nm thickness and ~40 nm diameter (Koester et al., 2008). In the gap regions of collagen fibrils, minerals nucleate to form intrafibrillar crystals, with the c-axis aligned with the molecule direction. These mineral particles grow and form plate-like crystals (Lees, 1979), as illustrated in Fig. 10a. These mineral particles undergo less strain than the fibrils; the fibril to mineral strain ratio is 5:2, and the collagen matrix must absorb the remaining three-fifths of strain (Gupta et al., 2006a, 2006b). Fig. 10a also shows interfibrillar minerals (between collagen fibrils) oriented with their c-axis perpendicular to the molecular direction. The mineralization on the outer surface of the fibrils forms a continuous network. Thus, both the mineral and the collagen form interpenetrating networks. This is only addressed by current models in a superficial manner. For instance, the Fratzl et al. (2004) model assumes platelets which are not interconnected. More research is needed, both experimental and computational, to develop a full understanding of the synergy between the two components. Buehler (2007) shows that, after initial slipping, mineralized collagen continues

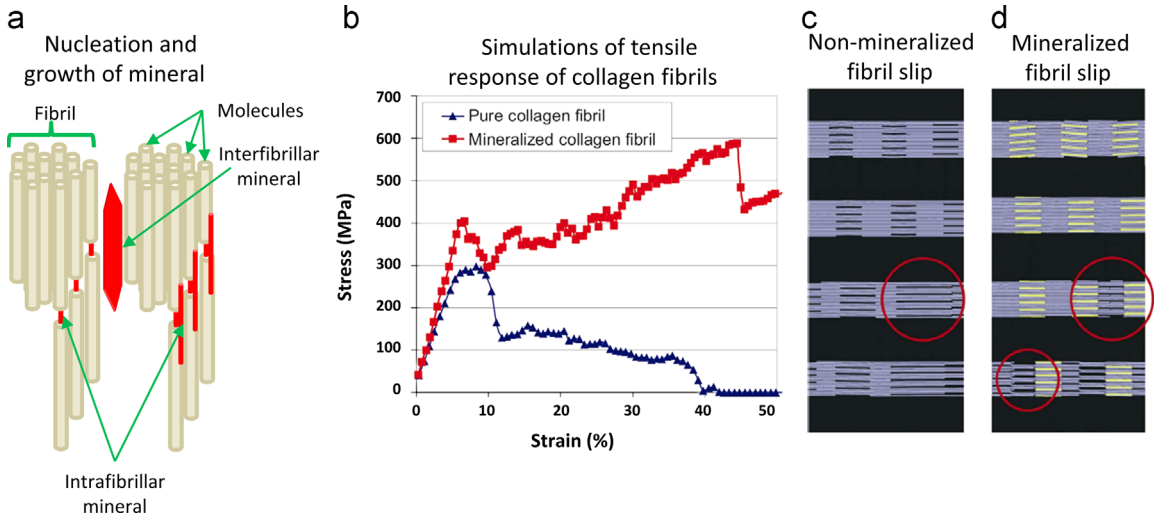

Fig. 10 – The effects of mineral on the collagen fibril. (a) Arrangement of mineral within and around collagen fibrils. Left: mineral nucleates in the gap region of fibrils. Right: nucleated mineral grows to form plate like crystals. Interfibrillar mineral grows between the two fibrils. (b) Simulations of the tensile stress–strain curves of non-mineralized and mineralized collagen fibrils. (c) Location of intermolecular slip of non-mineralized collagen. (d) Location of slip between mineral and collagen molecules (Buehler, 2007).

Please cite this article as: Sherman, V.R., et al., The materials science of collagen. Journal of the Mechanical Behavior of Biomedical Materials (2015), http://dx.doi.org/10.1016/j.jmbbm.2015.05.023

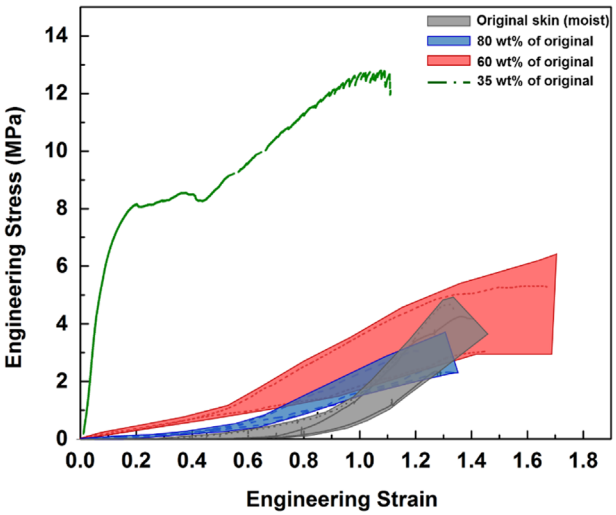

Fig. 11 – Stress–strain curves of original moist skin and dehydrated skin of different amounts. As skin becomes dehydrated, the toe region becomes shorter and stiffer due to increased adhesion between fibrils which prevents sliding and reorientation. After losing 65% of its weight to dehydration, the characteristic toe region of skin has vanished and been replaced with a higher stress quasi-toe region, which occurs when the internal stress is sufficient to break the bonds between dry fibrils and the fibrils proceed to reorient.

to carry a significant load compared to non-mineralized fibrils (Fig. 10b). The differences arise because non-mineralized collagen fibrils yield primarily by intermolecular slip (Fig. 10c). The slip leads to the deformation of the region with lower material density, initiating at the interface between mineral particles and collagen molecules, thus reducing the density of the material and inducing nanoscale voids (Fig. 10d). Via this nano-mechanism, the mineralized collagen fibrils are able to tolerate a large fraction of microcracks, without causing any macroscopic failure of the bone. In a way, the bone is remodeling itself (Buehler, 2007). Additionally, the formation of microcracks generates the mechanisms of 'crack meandering' and 'crack bridging' which enhance its toughness. The toughening mechanisms will be further discussed in Section 7.

3.6. *Effects of hydration*

The cross-linking of collagen fibrils is extremely important in establishing the mechanical response. In this regard, hydration plays a major role; in hydrated collagen, hydrogen bonds form between collagen and water, which allows for slipping and movement. However, as the collagen is dried, bonds form directly between collagen molecules and fibrils, preventing sliding and stiffening the structure. Skin is a suitable material to observe the effects of hydration; as the skin is dehydrated, its mechanical response is drastically changed, because of the reduction of interfibrillar sliding. The effect of dehydration was evaluated (Yang et al., 2015) by recording the stress–strain curves of skin after drying. The hydrated curve displays a long toe region; with dehydration, it becomes progressively shorter and stiffer. Four levels of hydration are shown in Fig. 11 (Yang et al., 2015), corresponding to the percentages of initial weight: 100, 80, 60 and 35%. The first corresponds to fresh skin which has a water content of approximately 65–70%. The skin containing 35% of the original weight has very little moisture content since, as noted earlier, collagen represents approximately 30% of the body weight in vertebrates.

The toe region of the stress–strain curve of skin shown in Fig. 11 is caused by the sliding and reorienting of collagen fibrils, which allows for large extension without high stress. The stress–strain curve of the most severely dried skin in this work (35 wt% of the fresh skin, or 65% weight reduction from fresh skin) does not show an initial toe region because the sliding between the collagen fibrils is highly limited due to the lack of water molecules. A plateau can be seen at 8 MPa, where the internal stress is sufficient to break the interfibrillar bonds and at which point fibrillar reorientation can occur. Therefore, an elevated stress toe-like region exists as the interfibrillar bonds begin to break. Modeling by Gautieri et al. (2012) predicts a decrease of the intermolecular separation from 1.6 to 1.1 nm with dehydration and, similarly, decreased intermolecular sliding in the collagen. In their computations, the force to pull a molecule from a microfibril increased from 4 nN to 30 nN. This calculated eight-fold increase is reflected in the higher stress levels measured with decreasing hydration.

4. Models for collagen extension (tensile response)

The mechanical properties of collagen and collagen-based tissues have been modeled using several approaches: (a) hyperelastic macroscopic models based on strain energy in which strain energy functions are developed and lead to mechanical behavior calculations, (b) macroscopic mathematical fits where a nonlinear constitutive equations are used, and (c) structurally and physically based models where a constitutive equation of a linear elastic material is modified by geometric characteristics. These models are necessary for collagen-based materials which undergo large deformations in order to capture their unusual mechanical behavior, which differs from the typical linear response of engineering metals and ceramics.

4.1. *Hyperelastic macroscopic models based on strain energy*

Strain energy models calculate stress in a material by taking the derivative of W, the strain energy, which is a function of the strain. Several models have been proposed for biological tissues including one by Fung (1993), developed specifically for skin; and more general models by Blatz et al. (1969) and Veronda and Westmann (1970). Stress vs. strain relationships can be derived from these models using assumptions such as incompressibility (Eq. (1)), assumed boundary conditions, and the relationship between stress and the strain energy (Eq. (2)). σ_1, σ_2, σ_3 represent the stresses, and λ_1, λ_2, λ_3 are the stretch ratios in the principal directions OX_1, OX_2, and OX_3.

The constancy in volume hypothesis is:

$$\lambda_1\lambda_2\lambda_3 = 1 \tag{1}$$

The difference in Cauchy stresses in principal directions is the derivative of the strain energy with respect to the direction of extension (the derivation is presented in the Appendix). This relationship results from a simplification of the Cauchy stress and strain energy relationship (Ogden, 1984). The result is Eq. (2).

$$\sigma_1 - \sigma_3 = \lambda_1 \frac{\partial W(\lambda_1, \lambda_2)}{\partial \lambda_1} \tag{2}$$

Tong and Fung (1976) developed a relationship between the strain energy and stress state, specifically for skin, as follows in Eq. (3). This "biphasic" function has two parts: the second term expresses the response at higher stress levels, while the first term represents the lower stress levels. Constants α, a, and c are used, and E_{ij} is the Green strain tensor.

$$W = f(\alpha, e) + c \exp[F(a, e)] \tag{3}$$

$$f(\alpha, e) = \alpha_1 E_{11}^2 + \alpha_2 E_{22}^2 + \alpha_3 E_{12}^2 + \alpha_3 E_{21}^2 + 2\alpha_4 E_{11} E_{22} \tag{4}$$

$$F(\alpha, e) = a_1 E_{11}^2 + a_2 E_{22}^2 + a_3 E_{12}^2 + a_3 E_{21}^2 + 2a_4 E_{11} E_{22} \tag{5}$$

where

$$E_{11} = E_1 = \frac{1}{2}(\lambda_1^2 - 1) \text{ and } E_{22} = E_2 = \frac{1}{2}(\lambda_2^2 - 1)$$

Blatz et al. (1969) suggested the relationship shown in Eq. (6), by modifying an equation originally proposed by Valanis and Landel (1967) and specifically applying it to soft tissues:

$$W = \sum_{i=1}^{3} C\left[e^{\alpha(\lambda_i^2 - 1)} - 1\right] \tag{6}$$

where C and α are constants

Veronda and Westmann (1970) developed the relationship for strain energy of the incompressible material shown in Eq. (7). However, this expression presupposes isotropy, limiting the generality. C_1, C_2, and β are constants used.

$$W = C_1\left[e^{\beta(I_1 - 3)} - 1\right] + C_2(I_2 - 3) \tag{7}$$

$$I_1 = \lambda_1^2 + \lambda_2^2 + \lambda_3^2 \text{ and } I_2 = \lambda_1^2\lambda_2^2 + \lambda_2^2\lambda_3^2 + \lambda_3^2\lambda_1^2 \tag{8}$$

I_1 and I_2 are the first and second strain invariants.

4.2. *Macroscopic mathematical fits*

Mathematical models make use of nonlinear constitutive equations to represent the extension of the skin. These models are not reduced to a strain energy form and do not represent the anisotropic three-dimensional stress state. Over the years, many relationships have been developed, using a variety of fitting parameters including a, b, d, k, C, n, β, α, and some physically based parameters such as σ^* (reference stress) and ε^* (reference strain), and physical inputs ε (strain) and σ (stress). Hyperbolic, exponential, and power equations have been used to describe the non-linear behavior. The first relationship was developed by Wertheim (1847) who proposed Eq. (9), a hyperbolic relationship between stress and strain:

$$\varepsilon^2 = a\sigma^2 + b\sigma \tag{9}$$

This expression gives a slope that monotonically increases with strain. Thus, over 150 years ago the response triggered the imagination of researchers. Fig. 12a shows the graphical representation of Wertheim's equation, given here because of its historical value. The parameters a and b are experimentally matched to the data.

Morgan (1960) and Ridge and Wright (1964) both proposed power relationships, Eqs. (10) and (11), respectively:

$$\sigma = \varepsilon^d \tag{10}$$

$$\varepsilon = C + k\sigma^b \tag{11}$$

An exponential stress strain relationship was specifically developed for biological materials, by Fung (1967):

$$\sigma = (\sigma^* + \beta)e^{\alpha(\varepsilon - \varepsilon^*)} - \beta \tag{12}$$

Fung (1967) suggested that the increase in slope experienced at higher strains is due to full extension of collagen and elastin fibers, and effectively applied his model to the rabbit mesentery. Fig. 12b shows the application of the Fung equation to dog aorta.

In general, the power law relationship is more effective at describing tissues with a larger toe region, as presented by Doehring et al. (2004). Recently, Chen et al. (2012) implemented a combined power law and linear equation using a

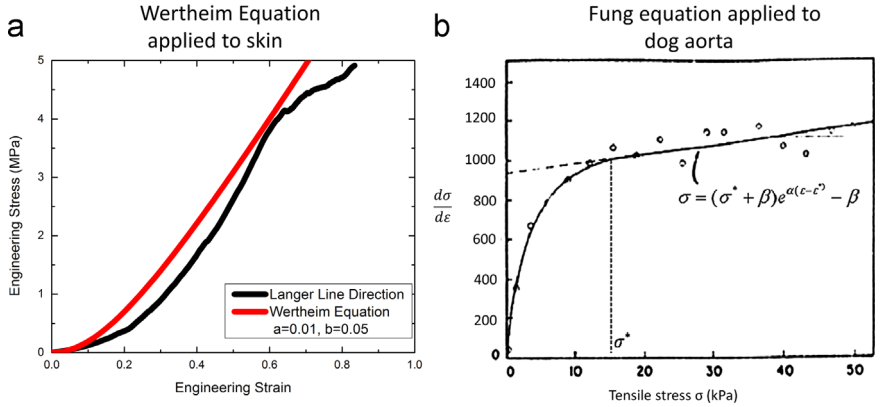

Fig. 12 – Wertheim and Fung equations applied. (a) Wertheim equation is applied to the skin extension curve along the Langer lines of a wild rabbit, or transverse to the direction of the body. (b) Representation of mechanical response of a dog aorta (circumferential strip) in terms of tangent modulus (slope of stress–strain curve) vs. tensile stress; slope and intercept provide parameters for Fung equation. (Reproduced based on Fung (1993)).

Please cite this article as: Sherman, V.R., et al., The materials science of collagen. Journal of the Mechanical Behavior of Biomedical Materials (2015), http://dx.doi.org/10.1016/j.jmbbm.2015.05.023

Heaviside function, as shown in Eq. (13). The unfurling and straightening of the polymer chains is described by the power law, followed by a linear region initiated by a Heaviside function and corresponding to the stretching of the polymer chain backbones:

$$\sigma = k_1 \varepsilon^{n \quad 1} + H(\varepsilon_c) E(\varepsilon - \varepsilon_c) \tag{13}$$

k, n, and ε_c are parameters and E is the slope of the linear portion. This equation shows a small discontinuity in slope at ε_c.

4.3. *Structurally and physically based models*

Structural models have been developed in order to describe the mechanical response of collagen as its configuration evolves under an applied strain. These models require the ability to observe how the structure of the fibers and fibrils evolves during extension. Some argue that the crimp structure of collagen has a two-dimensional wavy shape, while others state that it is a three-dimensional helix. Structural models have been developed to represent both assumptions. Due to the complexity of the collagen arrangements, the equations for these models are rather involved. The earliest model was proposed by Diamant et al. (1972), and is shown in Fig. 13a. Fibrils were modeled as in-plane zig-zag shaped beams, with fixed (and not jointed) apexes of infinite rigidity. Using the bending modulus of the beams between the apexes, the relationship between stress and strain takes the form of Eq. (14) where ε_∞ is the length of the fully extended fiber, E is the Young's modulus of the fiber, and λ is the total stretch ratio. A similar model was suggested by Markenscoff and Yannas (1979), who modeled collagen fibrils as hinged beams in order to estimate the onset of the heel region. The results were that for randomly oriented fibrils, alignment and stretching would occur at a strain of 0.57. Higher alignment leads to a reduction of the low stress region of the stress strain curve.

$$\varepsilon - (\sigma/E) = \varepsilon_\infty - \lambda\sqrt{(E/\sigma)} \tag{14}$$

In 1976, Comninou and Yannas (1976) developed a sinusoidal model for fibril shape, which was simplified in 1978 by Lanir (1978). The model is illustrated in Fig. 13b. Upon stretching, the energy of the system changes due to the tensile and bending deformation of fibers, matrix-fiber interactions (modeled as a beam on an elastic foundation) and the strength of elastin fibers. Lanir's equation is designed to include the elastic component of matrix fiber interactions, and takes into account both elastic and geometric strain of fibers, in the form of Eq. (15), where F_c is a horizontal component of force on the collagen fibers, ε_e is elastic strain of the fiber under extension (which is calculated using further equations), γ and α are geometric parameters, and K_e is the spring constant incorporating the cross sectional area:

$$F = F_c \varepsilon_e + K_e(\varepsilon_e + \gamma\Delta(\Delta + 2)/(1 + \Delta)^2) \tag{15}$$

where $\Delta = \alpha\varepsilon_e$.

A helical model was first developed in 1975 by Beskos and Jenkins (1975), but assumed fiber inextensibility—leading to an infinite stiffness at full extension. Therefore, this model was modified by Freed and Doehring (2005) to incorporate a piecewise function, allowing for a linear modulus at full fiber extension (denoted as $\bar{\lambda}$). The helical model is illustrated in Fig. 13c, and takes the form of Eqs. (16) and (17). Freed and Doehring (2005) used a strain energy function to calculate

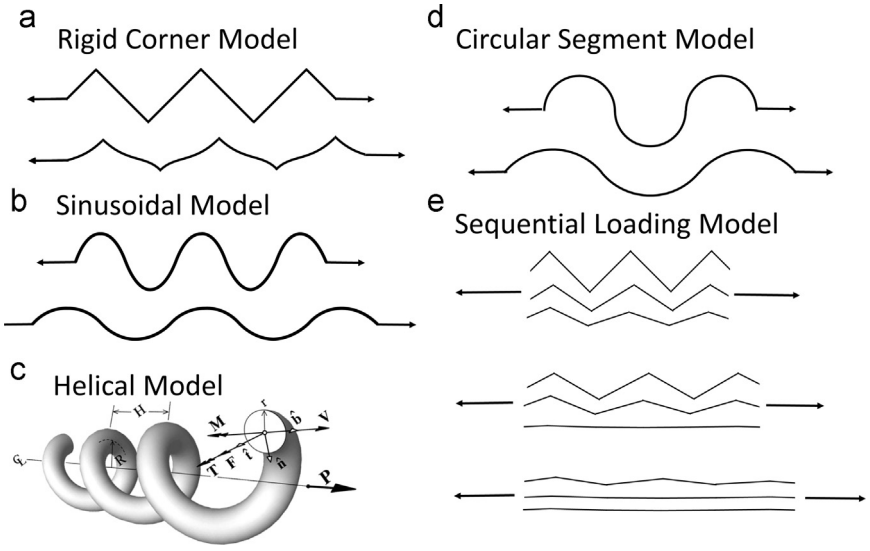

Fig. 13 – Structural collagen models and deformation. (a) The rigid corner model, assuming apexes of infinite rigidity. These apexes maintain their original angle under extension, while the beams in-between deform (Diamant et al., 1972). (b) The sinusoidal model, originally developed by Comninou and Yannas (1976), but later simplified by Lanir (1978). (c) The helical model, originally developed by Beskos and Jenkins (1975), and later modified for finite modulus at full extension by Freed and Doehring (2005). (d) Circular segment model, developed by Sherman et al. (2015) and first applied by Yang et al. (2015). (e) The sequential loading model developed by Kastelic et al. (1980), which assumes stiffness only due to fully straightened fibers.

Please cite this article as: Sherman, V.R., et al., The materials science of collagen. Journal of the Mechanical Behavior of Biomedical Materials (2015), http://dx.doi.org/10.1016/j.jmbbm.2015.05.023

stresses prior to full fiber extension, taking into account axial force, shear force, bending moment, and torque. $\overline{E}$ is a modulus based on the geometry of the helix, and ξ is a geometric parameter.

$$\text{For } \lambda < \overline{\lambda} \quad \sigma = \xi \overline{E}(\lambda - 1) \tag{16}$$

$$\text{For } \lambda > \overline{\lambda} \quad \sigma = \overline{E}(\overline{\lambda} - 1) + E(\lambda/\overline{\lambda} - 1) \tag{17}$$

Sherman et al. (2015) developed a model assuming that fibrils are circular segments of various radii and degrees of curvature, with the goal of most accurately reflecting the configuration of highly crimped fibrillar structures, as shown in Fig. 13d. Stresses are calculated through Eq. (18), while strains are obtained using Eq. (19). E' is a pseudo-modulus determined from the geometric shape, r is the radius of the circular segments, θ_0 is the initial angle of the circular segments, and r_c is the initial circle radius.

$$\frac{\sigma_0}{E} = \frac{1}{E} \cdot \int_{r_c}^{r} E' \left\{ \frac{\csc(\theta_0)}{r_c \cdot r} \left[r \sin\left(\frac{r_c}{r}\theta_0\right) - r_c\theta_0 \cos\left(\frac{r_c\theta_0}{r}\right) \right] \right\} dr \tag{18}$$

$$d\varepsilon = \left\{ \frac{\csc(\theta_0)}{r_c \cdot r} \left[r \sin\left(\frac{r_c}{r}\theta_0\right) - r_c\theta_0 \cos\left(\frac{r_c\theta_0}{r}\right) \right] \right\} dr \tag{19}$$

In 1980 Kastelic et al. (1980) took a different approach, suggesting that the variation in modulus is due to an assumption that resistance only arises from the elasticity of completely straight fibrils. Different degrees of crimp and variances in crimp angle affect the size of the toe and heel region. θ represents crimp angle of the outermost collagen fibrils in a fiber, $\theta(\rho)$ crimp angle at relative radius, ρ inside the fiber, R^* is fibril radius, and b represents a blunting factor, to reduce the sharpness of the crimps in the model which is shown in Fig. 13e and represented by Eq. (20).

$$\sigma/E = \varepsilon(R^*)^2 - 2(1-b)\int_0^{R^*} \left(\frac{1}{\cos\,\theta(\rho)} - 1 \right) \rho d\rho \tag{20}$$

The worm-like chain model derives a nonlinear constitutive equation based on a continuously flexible isotropic rod. One example of a rod like this is a noodle; an important parameter, the persistence length, is the length for which the correlations in the orientation of the two ends are lost. The worm-like chain model takes into account an entropic term (due to changes in configuration) as well as an enthalpic term (due to elongation of the polymer). Inputs into the model include force, F; the Boltzmann constant, k_b; the absolute temperature, T; the persistence length, L_p; the contour (total) length of the fibers, L; and z, the extension (displacement) (Bustamante et al., 1994; Meyers and Chen, 2014).

$$F = \frac{k_b T}{L_p} \left(\frac{1}{4(1 - z/L)^2} - \frac{1}{4} + \frac{z}{L} \right) \tag{21}$$

Four of the physically-based structural models presented can be compared to experimental observations, as shown in Fig. 14. It is clear that for the tendon to which these models are being compared, the sine wave and circular segment are the most plausible ones. It is important to consider that these curves are plotted under the assumption that sliding between fibrils does not occur and does not contribute to strain. In fact, any sliding will shift the curve towards the right. If sliding does occur during extension (and this is treated in Section 4.4), the circular segment model may be the most accurate representation of the in vivo fibrillar shape. This is also the most physically plausible configuration because the curvature is constant along the fiber length.

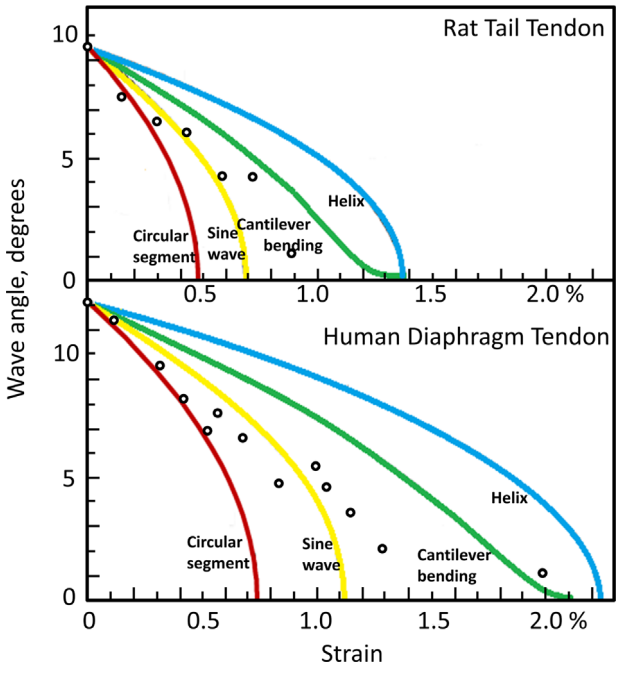

Fig. 14 – Comparison of wave angle under tension in different structural models. Experimental data points from tendon under tension (open circles) are compared to a calculated decrease in wave angle of structural models. In calculations, strictly geometric changes are accounted for; there is no inclusion of elastic strain or sliding, both of which are known to occur. Any elastic strain or sliding would add to the amount of strain at a particular stress level; the curves would be shifted towards the right. Adapted from Dale et al. (1972).

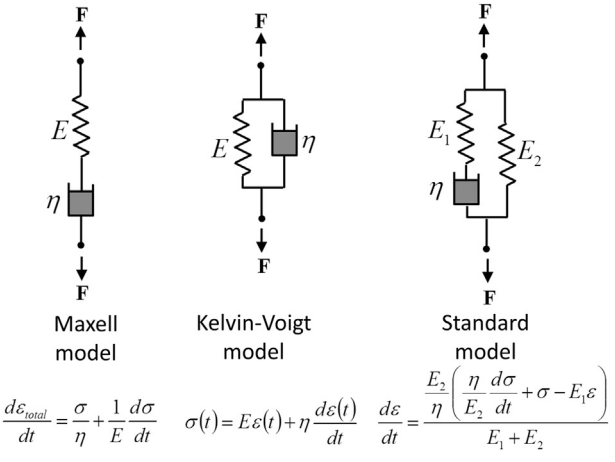

Fig. 15 – Viscoelastic models. Three common models for viscoelastic behavior, and corresponding equations in terms of stress and strain (Meyers and Chen, 2014).

4.4. *Viscoelasticity in collagen structures*

The theory of viscoelasticity is well established, the simplest representation of a viscous component being the dashpot. There are three principal models used to represent different viscoelastic materials, which consist of arrangements of springs and dashpots. These models are the Maxwell, Kelvin, and the Standard models. For the complete derivations, see, for instance, Meyers and Chen (2014). Fig. 15 shows the three models with their governing constitutive equations.

The amount of research on the viscous component of biological materials is rather limited. Puxkandl et al. (2002) modeled the collagen fiber as two Kelvin models in series. The first element in the series represents the fibril, with the viscous effects caused by molecular friction and the elastic component derived from molecular cross links. The second in

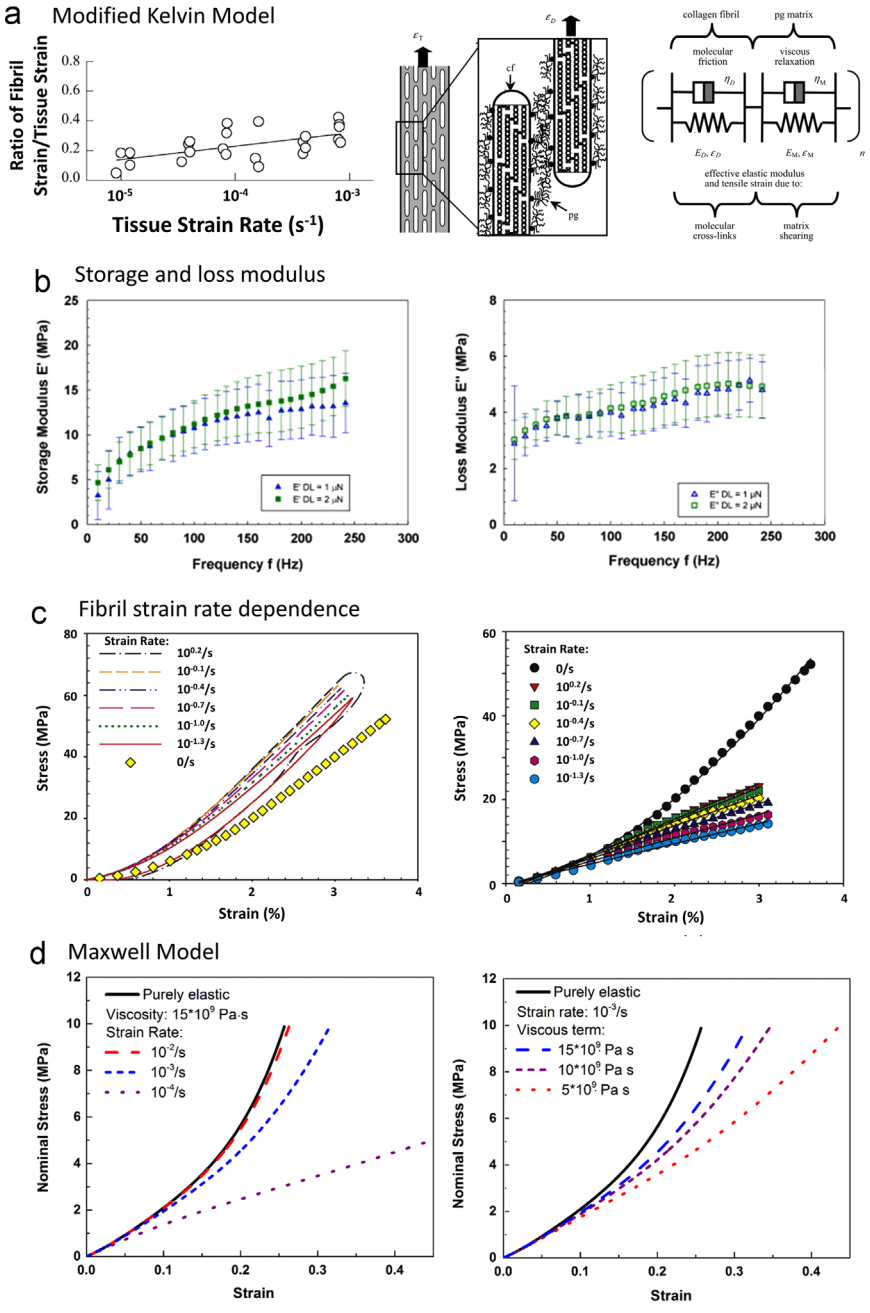

Fig. 16 – Modeling of viscoelasticity in collagen structures. (a) Puxkandl et al. (2002) used two Kelvin models, and showed that increased strain rate increased fibrillar strain relative to tissue strain. (b) Nanoindentation tests from Franke et al. (2011) show increase of storage and loss modulus with increased frequency. (c) Strain rate dependence of a collagen fibril by Svensson et al. (2010). Left: fibril pulled at different strain rates show the effects of viscosity. Right: Elastic curve (black) taken from near zero strain rate is subtracted from dynamic curves to show viscous component of fibril extension (all other colors). (d) Incorporation of viscosity and strain rate by Yang et al. (2015), holding representative viscosity constant (left) and holding strain rate constant (right).

Please cite this article as: Sherman, V.R., et al., The materials science of collagen. Journal of the Mechanical Behavior of Biomedical Materials (2015), http://dx.doi.org/10.1016/j.jmbbm.2015.05.023

the series represents the proteoglycan-rich matrix, with the viscous effects caused by proteoglycan viscous relaxation and the elastic component caused by matrix shearing. This in series Kelvin arrangement is described by Eq. (22), where α, β, and γ are defined material properties, ε_D is fibrillar strain, and ε_T is total strain.

$$\frac{d\varepsilon_D}{d\varepsilon_T} = \alpha + (\beta - \alpha) exp\left[-\gamma \varepsilon_T / \dot{\varepsilon}_T\right] \tag{22}$$

Using in situ X-ray diffraction, the elongation of collagen fibrils and the tendon as a whole were simultaneously measured (Puxkandl et al., 2002), and the viscous effects caused the ratio of fibrillar strain to tendon strain to increase with increased strain rates. Fig. 16a shows the model used, and the increasing ratio of fibrillar to total strain measured during tests.

The storage modulus (E') and loss modulus (E'') of articular porcine cartilage were measured using dynamic indentation in the range of 1–250 Hz by Franke et al. (2011); this frequency is representative of loading conditions in gait. E' describes the in-phase elastic response of a given material, and E'' is a measure for the damping/energy being dissipated throughout the experiment. Both were measured from the oscillations in the loading of a nanoindenter. The contact damping, D_c, frequency, ω, and contact stiffness, C are related to the storage and loss modulus through Eq. (23). The resulting measurements are shown in Fig. 16b; both storage and loss moduli are related to the loading frequency, reflective of the strain-rate dependence of collagenous materials. The trend is for both to increase with increasing loading frequency.

$$\frac{E'}{E''} = \frac{D_c \omega}{S} \tag{23}$$

Single human collagen fibrils were extracted from the patellar tendon by Svensson et al. (2010). Using AFM, tests were performed at multiple strain rates to distinguish the viscous and elastic components of the tensile response. The results, shown in Fig. 16c, are well fitted by a second order polynomial. Additionally, they show that viscosity is a decreasing function of the strain rate. This is in agreement with results of self-assembled fibers tested by Silver et al. (2002), who suggested that the thixotropic effects are due to interstitial water molecules which hydroplane on subfibrillar elements at increasing strain rates.

Yang et al. (2015) expressed the time-dependent component using the Maxwell model, with the elastic spring (Eq. (18)) and a dashpot in series. The viscous contribution is due to the time-dependent sliding between fibrils. The viscous term can be represented by a simple Newtonian response:

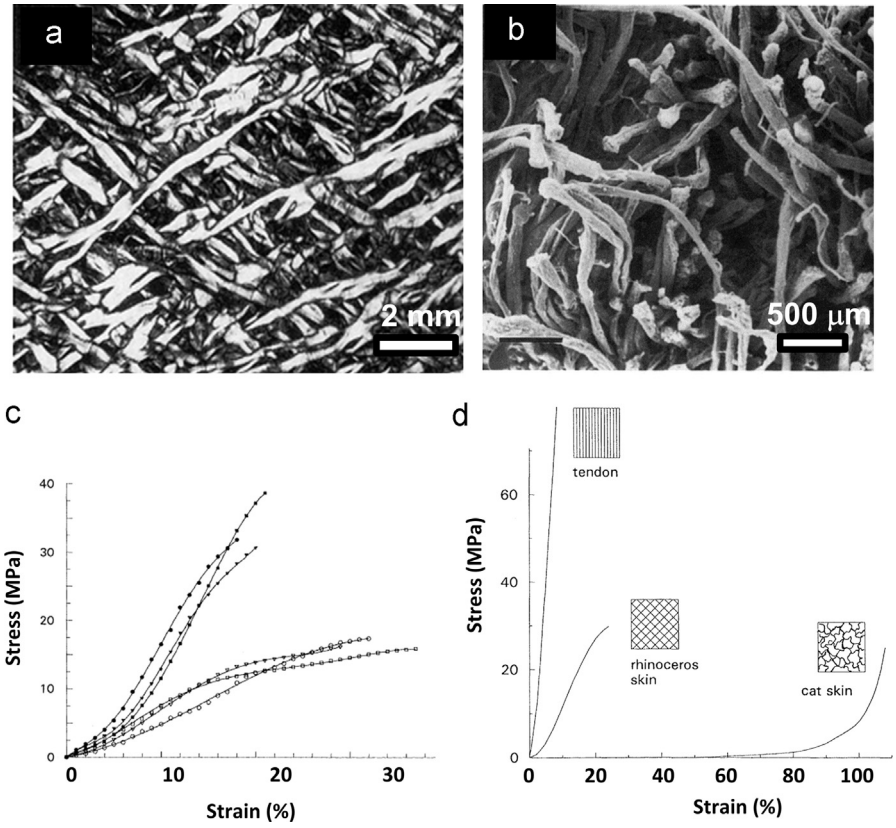

Fig. 17 – Microstructure and tensile response of a rhinoceros skin from Shadwick et al. (1992). (a) The rhinoceros skin displays a woven structure of collagen fibers. (b) Fracture of the rhinoceros skin reveals minimal waviness of the collagen fibers. (c) Tensile tests of three orthogonal directions of dorsolateral (stiffer, closed circles) and belly (open circles). Dorsolateral skin is substantially stiffer than belly skin, but orientation effects are insignificant. Due to the straight collagen fibers, rhinoceros skin exhibits a unique tensile response with a minimal toe region. (d) Tensile response of rhinoceros skin plotted next to cat skin in order to illustrate the relative inextensibility of rhinoceros skin.

Please cite this article as: Sherman, V.R., et al., The materials science of collagen. Journal of the Mechanical Behavior of Biomedical Materials (2015), http://dx.doi.org/10.1016/j.jmbbm.2015.05.023

$\sigma = \eta\dot{\varepsilon}_t$, where η is the Newtonian viscosity, such that the viscous strain is given by:

$$\varepsilon_\eta = \frac{1}{\eta}\int \sigma dt \tag{24}$$

For simplicity, a polynomial fit to the elastic constitutive equation of the form $\sigma = A\varepsilon_{el} + B\varepsilon_{el}^2 + C\varepsilon_{el}^3 + D\varepsilon_{el}^4$ is used, where A, B, C and D are fitting constants, which leads to:

$$\varepsilon_\eta = \frac{1}{\eta}\int (A\varepsilon_{el} + B\varepsilon_{el}^2 + C\varepsilon_{el}^3 + D\varepsilon_{el}^4)\dot{\varepsilon}^{-1} d\varepsilon \tag{25}$$

where $\dot{\varepsilon}$ is the strain rate. The viscous component comes from interfibrillar bonds, the breaking of which results in sliding between fibrils. Thus, the fractional area where viscous flow takes place is small; as such the viscosity used in Eq. (25) is an 'effective' viscosity. The elastic response is modified as a function of viscosity (at a constant strain rate) and strain rate (at a constant viscosity) in Fig. 16d. These calculations show in schematic fashion how the viscosity influences the mechanical response. As the samples dry, the viscosity increases and the overall response is altered.

The three cases above illustrate the incorporation of viscosity into the constitutive response. The sliding component is very important and cannot be ignored.

5. Collagen in skin

Collagen has a specialized hierarchical structure in skin. The structure of skin varies greatly between different species, because of the functional requirements of the specific species of animal. However, skin is generally regarded as an anisotropic, nonlinear elastic material. By investigating the skin of various animals, we can observe important differences in the structures due to evolutionary constraints, which lead to unique mechanical properties. The structural features and mechanical response of the skin of three widely different vertebrates, the rhinoceros, rabbit, and chicken are summarized in Figs. 17–19.

5.1. *Rhinoceros (Ceratotherium simum)*

The rhinoceros is a fighting animal, and its skin is adapted accordingly. A tightly woven structure (Fig. 17a) of collagen fibers creates a thick dermis which, due to the abnormally straight collagen fibers (Fig. 17b), lacks the large toe region typical of most mammalian skin (Fig. 17c). This arrangement leads to a response which is directionally isotropic, and lacks the extreme tear resistance common to most skins. While this may first seem to be a disadvantage for a fighting animal, it is not the case. Were the skin to be punctured (as is

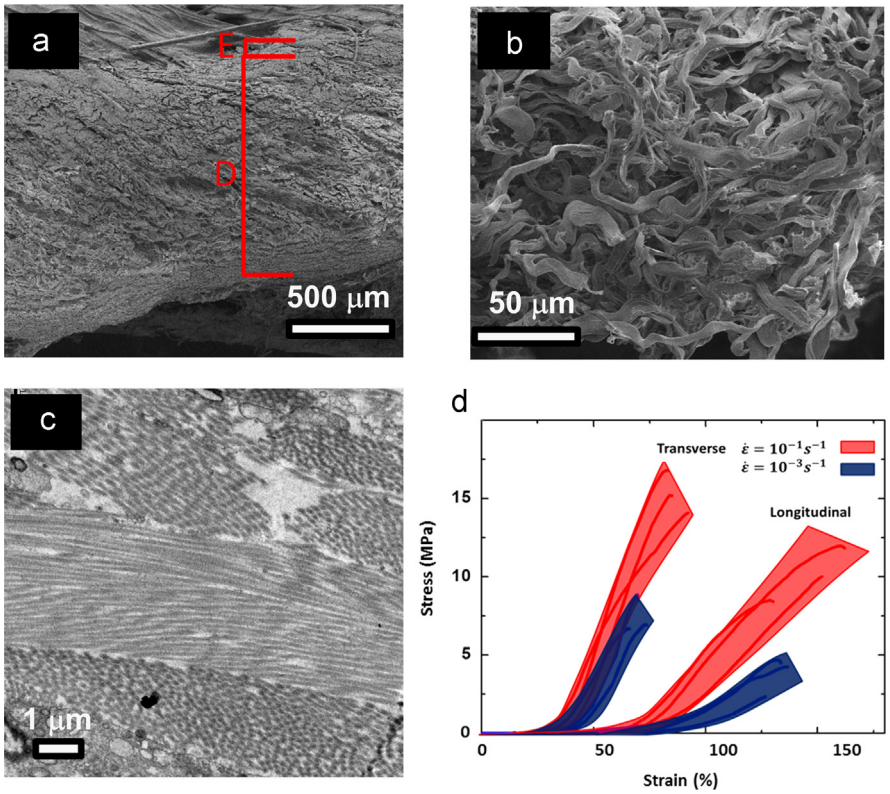

Fig. 18 – Microstructure and tensile response of rabbit skin. (a) Rabbit skin epidermis (E) and dermis (D). Compared to epidermis, dermis is much thicker and made of a network of intertwined wavy collagen fibers. (b) Close examination of a fracture surface reveals an extremely wavy structure. (c) TEM of rabbit skin cross section shows several fibers in different orientations. (d) The wavy structure of rabbit skin collagen leads to a large toe region under tension, as shown by Yang et al. (2015). Additionally, the skin shows highly anisotropic testing results, suggesting that the collagen fibers lie principally in certain preferred orientations.

Please cite this article as: Sherman, V.R., et al., The materials science of collagen. Journal of the Mechanical Behavior of Biomedical Materials (2015), http://dx.doi.org/10.1016/j.jmbbm.2015.05.023

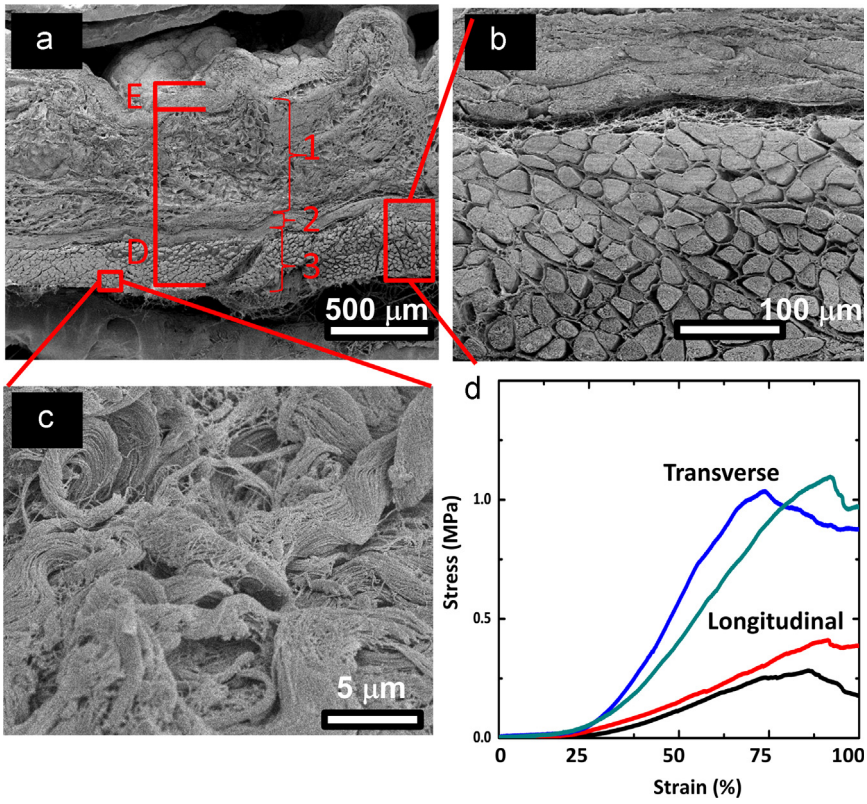

Fig. 19 – Microstructure and tensile response of chicken skin. (a) Chicken skin epidermis (E) and dermis (D). The dermis consists of three distinct layers (1, 2, 3 in figure); layer 1 is a spongy arrangement of collagen fibers, while layers 2 and 3 consist of densely packed collagen fibers which are packed into fascicles. (b) The fascicles in layers 2 and 3 viewed at higher magnification. (c) Fracture surface showing wavy fibers which fascicles are made of. (d) Tensile response in the transverse and longitudinal directions is drastically different due to the minimal interaction between the two layers of fascicles.

inevitable in a fight) but not tear, the energy of the blow would focus on the penetration region, and put the major organs of the animal at risk. By tearing, the rhinoceros is subjected to superficial gashes but the energy from the blow is dissipated across a larger area while avoiding deeper penetration which could lead to lethal damage. This design is different from other mammalian skin, which has a larger toe region in order to absorb strain energy and prevent fracture altogether. For comparison, the response of the rhinoceros skin alongside the response of cat skin is shown in Fig. 17d. The skin of the rhinoceros is highly cross-linked and stronger than most, with a failure strength of ~35 MPa and relatively low fracture strains of ~0.2 on most of the body, and slightly over 0.3 on the belly (Shadwick et al., 1992).

5.2. *New Zealand white rabbit (Oryctolagus cuniculus)*

In opposition to the rhinoceros, the New Zealand (NZ) white rabbit has a skin with radically different mechanical response. This small creature needs skin which will not tear as it crashes through sticks and branches. Therefore, it has a microstructure which is much different than that of the rhinoceros; the NZ white rabbit's skin is a vast meshwork of wavy collagen fibers (Fig. 18a and b), which TEM reveals to lie in-plane with the skin (Fig. 18c). This is a transmission electron micrograph of a thin section showing a fiber horizontally bisecting the picture with fibrils close to parallel to the foil plane, while the top and bottom portions reveal the cross sections of the fibrils and fibers. This shows that the fibers have a range of different orientations, consistent with Fig. 18b. A larger dermis and a comparatively thin epidermis cause the mechanical properties to be dominated by the dermis. Upon extension, the fibers undergo significant straightening and reorientation, allowing the skin to experience large strains with very little stress. This response is captured well by the model of Sherman et al. (2015) in which the radius of the circular section gradually increases. Under further extension, all fibers become straight and aligned, at which point the slope of the stress strain curve increases rapidly, and stresses begin to rise linearly with strain (Fig. 18d). Throughout the extension process, fibril straightening, reorientation, stretching and sliding all contribute to a skin which sacrifices some strength compared to that of the rhinoceros, but is demonstrated to be extremely tear resistant. Additionally, as seen in Fig. 18d, the rabbit skin is highly anisotropic; this is due to geometric effects and initial fiber orientations in the skin structure. The fracture strength of rabbit skin is ~12 MPa, at strains in excess of 0.5 and up to 1.5, parallel and perpendicular to the Langer lines (Yang et al., 2015; Lanir and Fung, 1974). These lines define the stiffest direction in the skin.

Please cite this article as: Sherman, V.R., et al., The materials science of collagen. Journal of the Mechanical Behavior of Biomedical Materials (2015), http://dx.doi.org/10.1016/j.jmbbm.2015.05.023

5.3. *Chicken (Gallus gallus)*

The skin of the brown chicken has another type of unique structure and function. Chicken skin supports the feathers, which also protect it from predators. The chicken neck skin was observed in these experiments. While in most animals the dermis is thick and compact, in the chicken a thick spongy layer provides the site for anchoring the roots of the feathers (calami). Beneath the spongy dermis lies a compact dermis which consists of two distinct layers of densely packed collagen fascicles, each with a clearly visible preferred orientation (Fig. 19a). Fascicles consist of wavy fibers, which contribute to the large toe region of chicken skin in tension (Fig. 19b and c). The thicker layer of the dermis is oriented in the direction along which strength is more crucial for the support of the feathers. This structure of multiple layers with minimal interactions, as well as a large epidermis sacrifices the strength of the skin; the fracture strength of the skin is orientation dependent (according to whether the thicker or thinner layer of the dermis is aligned with the tensile stress) and ranges from ~0.5 to 1.0 MPa, at strains of ~0.8–1.0 (Fig. 19d).

6. Collagen in fish scales

The refined structural design of collagen in fish scales facilitates a robust armor tailored to the needs of the particular species. Fish with unique requirements have evolved different types of scales and mechanisms in order to provide protection from predators. Scales can be classified into several distinct types: ganoid, elasmoid, placoid, cycloid, cosmoid and ctenoid. Three chosen scales are described here: the ganoid scale of the alligator gar, the elasmoid scale of the arapaima, and the cosmoid scale of the coelacanth.

6.1. *Alligator gar (Atractosteus spatula)*

The ganoid scales of the alligator gar are thick and have a highly mineralized exterior surface with a tough, boney foundation (Fig. 20a and b). In Fig. 20a, the ganoid surface layers is white, whereas the bone is darker. The cross section, shown in Fig. 20b, shows a serrated interface between the two layers whose function is possibly to increase adhesion and crack deflection ability. These penetration-resistant scales are necessary to provide protection from the alligator, as well as from self-predation. To achieve this, a mineralized matrix of collagen fibrils with parallel tubules throughout provides a tough, crack impeding foundation (Fig. 20c) of ~3.5 mm thick in adult fish. An outer mineralized surface of ~1.5 mm, called ganoine, is nearly pure hydroxyapatite and covers a large percent of the scale. The ganoine provides a hard (2.5 GPa microhardness) barrier against penetration by teeth; beneath it, the softer (400 MPa microhardness) but tougher bone-like base consisting of a hydroxyapatite and collagen composite provides flexural strength. This robust scale is highly

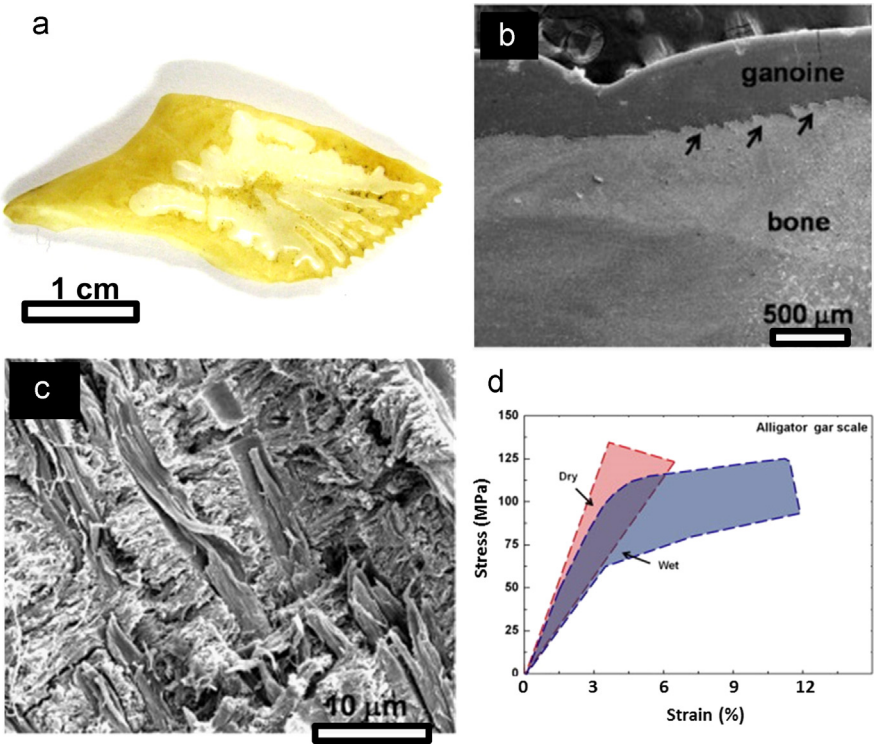

Fig. 20 – Microstructure and tensile response of alligator gar scale. (a) The entirety of the ganoid type alligator gar scale. Lighter area is exposed ganoine, while darker area is boney base. (b) Cross-section of gar scale. Two distinct layers; highly mineralized external ganoine layer, and boney base layer. (c) Fracture surface of boney layer of gar scale made up of hydroxyapatite crystals and mineralized collagen, with small tubules which run from the scale base to the ganoine layer. (d) Tensile response of gar scale. High degree of mineralization minimizes effects of hydration, prior to yielding. However, a large amount of deformation is attainable post-yield when testing hydrated samples, due to the large elasticity of wet collagen fibrils.

Please cite this article as: Sherman, V.R., et al., The materials science of collagen. Journal of the Mechanical Behavior of Biomedical Materials (2015), http://dx.doi.org/10.1016/j.jmbbm.2015.05.023

protective, but not flexible. Due to mineral protein interactions which reduce collagen sliding, hydration (or lack thereof) has minimal effects on the modulus of the gar scale. However, hydration does cause a large degree of post-yield plasticity (Fig. 20d). In order for the fish to remain flexible at a low weight penalty there is a small overlap, ~30% across scales. The scales are able to move with hinge like interfaces in the required directions and allow for flexibility, required for propulsion. This unique tridimensional arrangement provides a protective layer of constant thickness (Yang et al., 2013a,b). The Senegal bichir, although a fraction of the size (2–3 m vs. 0.1–0.5 m length), has scales with a similar architecture and materials structure.

6.2. *Arapaima (Arapaima gigas)*

The arapaima is a teleost fish which has elasmoid scales specialized for protection against the piranha (Yang et al., 2014). Similar to the gar and most other fish species (Zhu et al., 2012), the arapaima scale (Fig. 21a and b) has an external layer (microhardness: 550 MPa) that is harder than the internal layers (200 MPa) (Lin et al., 2011). However, these values are much lower than the ones of ganoid scales. In the arapaima, lamellae of parallel collagen fibrils beneath the hard mineral external layer form a Bouligand-like structure, shown in Fig. 21c. These lamella slide across each other to allow flexibility. Due to the high collagen content of the arapaima scale, the hydration levels are crucial to their function. Fig. 21d shows that without hydration, the collagen layers cannot slide, the elastic modulus is much higher, and the scale toughness (area under the stress–strain curve) decreases. For the arapaima, a flexible scale is necessary due to the large degree of overlap, which is in excess of 60% (Yang et al., 2014). With large scales ~8 cm in length and a large degree of overlap, scale flexibility is required. Otherwise, the scales would be unable to conform to the fish's body as it flexes during motion, and the protective nature of the scales would be compromised. In the natural hydrated state, the outer mineral layer provides hardness, minimizing local plasticity and promoting fracture of the piranha tooth. As deformation continues, the inner collagen is able to bend, deform, and rotate, supporting larger amounts of plastic deformation while averting failure.

The Bouligand-type structure of the teleost fish renders propagation of a crack very difficult for two principal reasons: a) A crack cannot propagate along a simple path because successive layers of collagen have different orientations and therefore the front is delocalized. b) The delamination of fibers and their defibrillation at the front of a crack creates a process zone, since fibrils connecting the opposite sides generate compressive stresses at the crack tip. Fig. 22a–d shows images of the opening of a notch viewed in a scanning electron microscope with a tensile attachment. It was not possible to propagate the crack since the layers of collagen (four imaged) separated, stretched, rotated, and defibrillated. Dastjerdi and Barthelat (2014) developed a fracture toughness

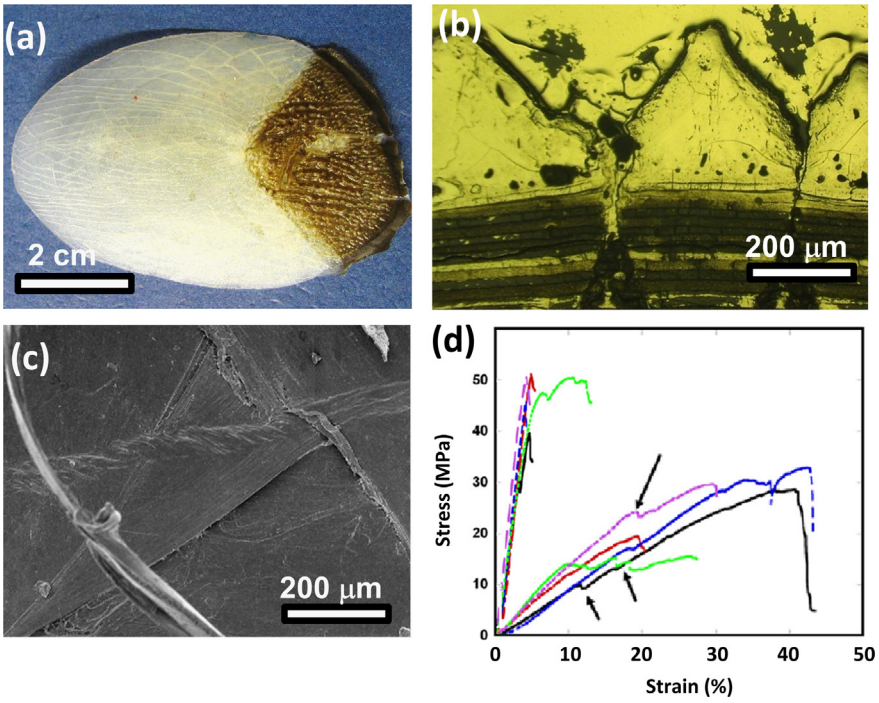

Fig. 21 – Microstructure and tensile response of arapaima scale. (a) The entirety of the arapaima scale. (b) Cross-section of arapaima scale; there are many layers including a thick ridged external mineral layer, and many thinner collagen layers beneath. (c) View of the multiple orientations of several internal collagen layers. View is perpendicular to the surface of scale. (d) Testing of arapaima scale. Due to low degree of mineralization, hydrated fibrils easily slide across one another. Therefore, wet scales are much more ductile than dry scales. Additionally, it is clear that the wet scales fail in stages, as individual layers of collagen fail. A previous study by Yang et al. (2014) has illustrated a complex process of failure avoidance, including stretching, rotation and delamination of collagen layers.

Please cite this article as: Sherman, V.R., et al., The materials science of collagen. Journal of the Mechanical Behavior of Biomedical Materials (2015), http://dx.doi.org/10.1016/j.jmbbm.2015.05.023

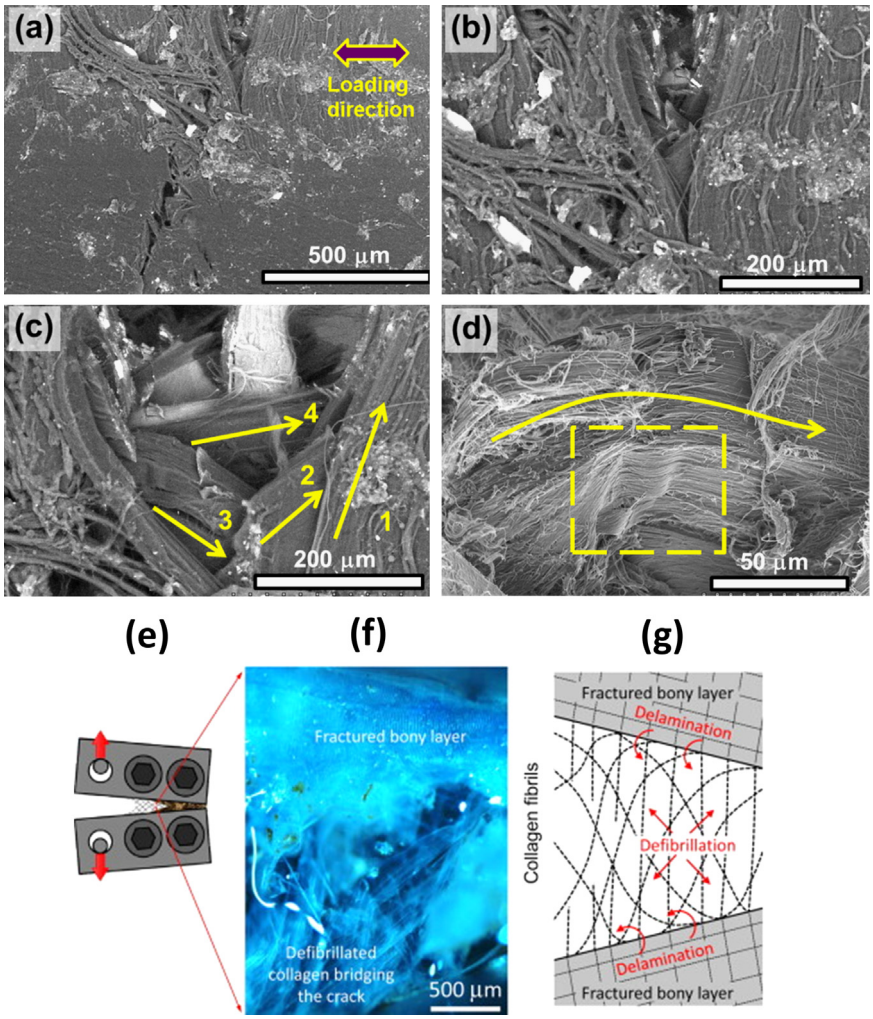

Fig. 22 – Extraordinary resistance to damage propagation in scale of teleost fish. (a-d) *Arapaima gigas*; **(e-g)** *Moronis saxitilis* **(a) Initial configuration of notch at the onset of loading (the notch is in the center of the image with the notch root pointing towards the bottom); (b) the collagen fibrils separate when the samples are being loaded; (c) four orientations of lamellae are being exposed (shown by the individual arrows); (d) the collagen fibrils bend and stretch as shown by the arrow; some of the collagen fibrils relax when the test stopped (Yang et al., 2014) (e) fracture toughness testing configuration; (f) defibrillated collagen fibrils; (g) schematic mechanism showing how delamination and defibrillation of fibrils leads to formation of extensive process zone (from Dastjerdi and Barthelat (2014)).**

testing setup (Fig. 22e) for the scales of *Moronis saxitilis* (striped bass) and obtained values of 15–18 kJ/m^2. This places scales, according to Dastjerdi and Barthelat (2014), at the top of the Wegst-Ashby toughness chart, above all other biological materials. The intricate mechanism by which a process zone develops is shown in Fig. 22f and drawn schematically in Fig. 22g. The bony layer contributes little to the toughness and fractures readily, as was also shown by Yang et al. (2014). The delamination of fibers and their separation into fibrils creates a process zone at the tip of the crack and effectively impedes its propagation.

The mechanism of fibril, stretching, rotation, and delamination can be modeled by molecular dynamics, using the coarse graining methodology which allows larger molecules to be simulated. The molecular dynamics model, based on a simple elastic network model (Qin and Buehler, 2011, 2013), was used to theoretically investigate the mechanisms of the deformation and delamination in the Arapaima scales under uniaxial tension. This model does not take the fibrils as elements but rather considers the larger collagen fibers to better simulate the response of the lamellae.

Molecular dynamics methods were applied to a scale consisting of 3 lamellae, which is shown in Fig. 23. In order to determine the correct surface energy of the collagen fibers in the scale, multiple simulations were run. These simulations, shown in Fig. 23b reveal that 1 J/m^2 provides the best approximation to the stress–strain curve of the scales shown in Fig. 21d. The deformation of the individual lamellae during the simulation reveal collagen bridging, delamination, and sympathetic lamella rotation.

6.3. *Coelacanth (Latimeria chalumnae)*

The coelacanth is considered a living fossil. It evolved 400 million years ago and was considered extinct until it was

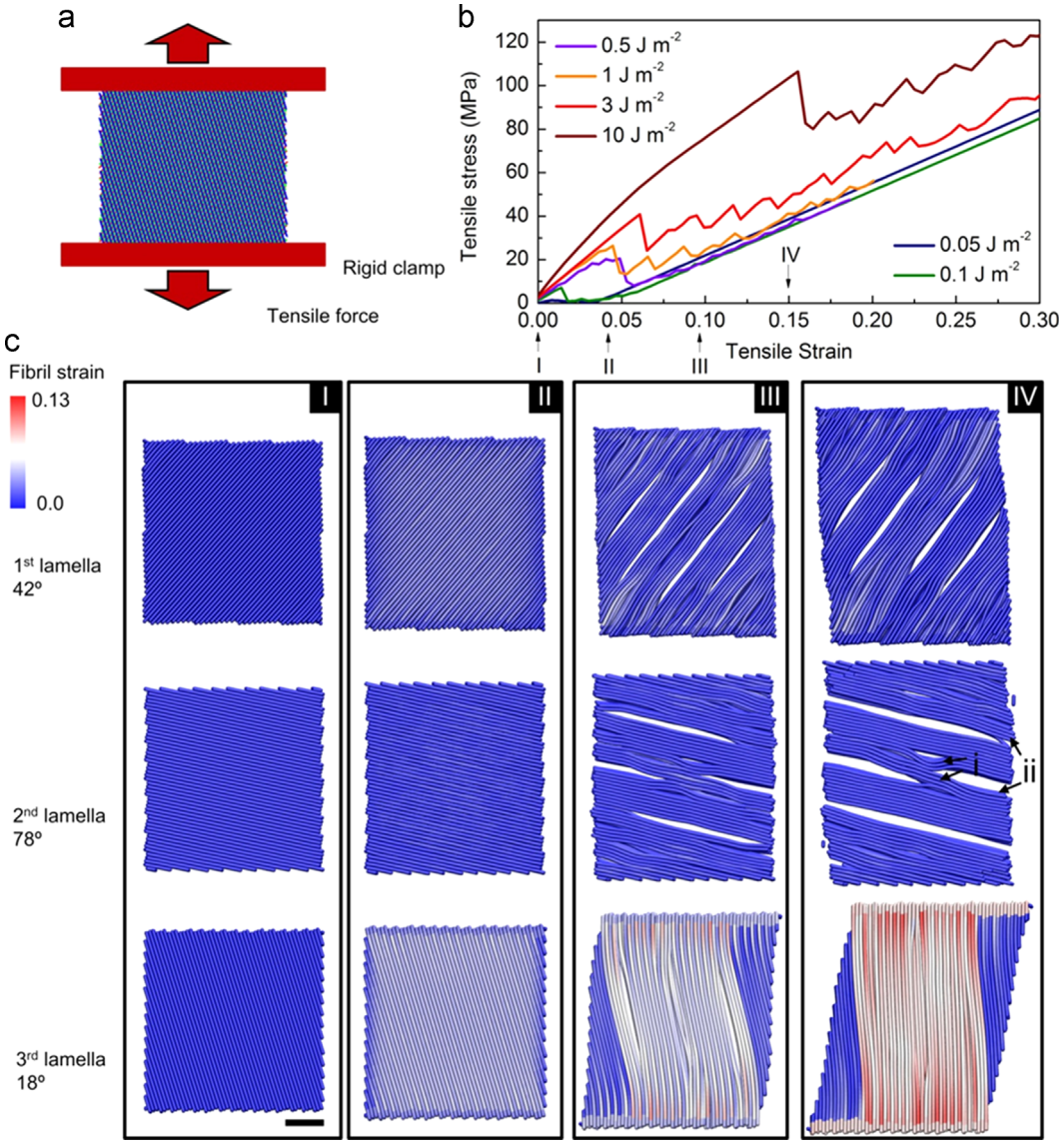

Fig. 23 – Molecular dynamics applied to the arapaima scale by Yang et al. (2014). Collagen lamellae are modeled as three layers oriented at different angles to the tensile direction. (a) Schematic of the scale as modeled for MD simulations. (b) Stress–strain curves for different surface energies. 1 J/m^2 gives the best approximation to the experimental stress–strain curve shown in Fig. 21d. (c) Simulation snapshots of the deformation of each lamella, taken at increasing strains of 1%, 4%, 9% and 15% (I, II, III, and IV marked in b). Molecular dynamics confirms the mechanical test observations: collagen bridging (noted by i), delamination (noted by ii), rotation, and stretching, which is shown for the 18° lamellae at a strain of 14% (red gradient in model). Scale bar: 10 μm. (For interpretation of the references to color in this figure legend, the reader is referred to the web version of this article.)

rediscovered in 1938 close to Madagascar. It is related to lungfish, reptiles, and mammals, and has vestigial limbs that come from their terrestrial ancestors. It belongs to the Latimerioidei suborder and is one of the few living fish with cosmoid scales, the other being the Australian lungfish. Thus, its unique structure is of great interest; the only study, to the authors' knowledge, is due to Giraud et al. (1978). The structure of the coelacanth scale, that is being correlated to its mechanical response by Quan et al. (2015), is shown in Fig. 24a. The degree of overlap is quite high, as measured by the covered area/total area ratio of 0.80. The degree of imbrication is correspondingly low (exposed length/total length): 0.32. These values compare with the arapaimas which has a 0.75° of overlap and a degree of imbrication of 0.4.

The cross section of the scale, viewed by the inclined view in Fig. 24b and from the perpendicular direction in Fig. 24c, reveals the external layer which is highly mineralized and the foundation consisting of parallel lamellae connected by struts. The collagen lamellae are organized into fiber bundles and these are comprised of fibrils. There is also separation between the fibers/bundles in the lamellar planes as shown in Fig. 24d. The angle between adjacent lamellae is close, but not equal to, 90°. This was identified by Giraud et al. (1978)

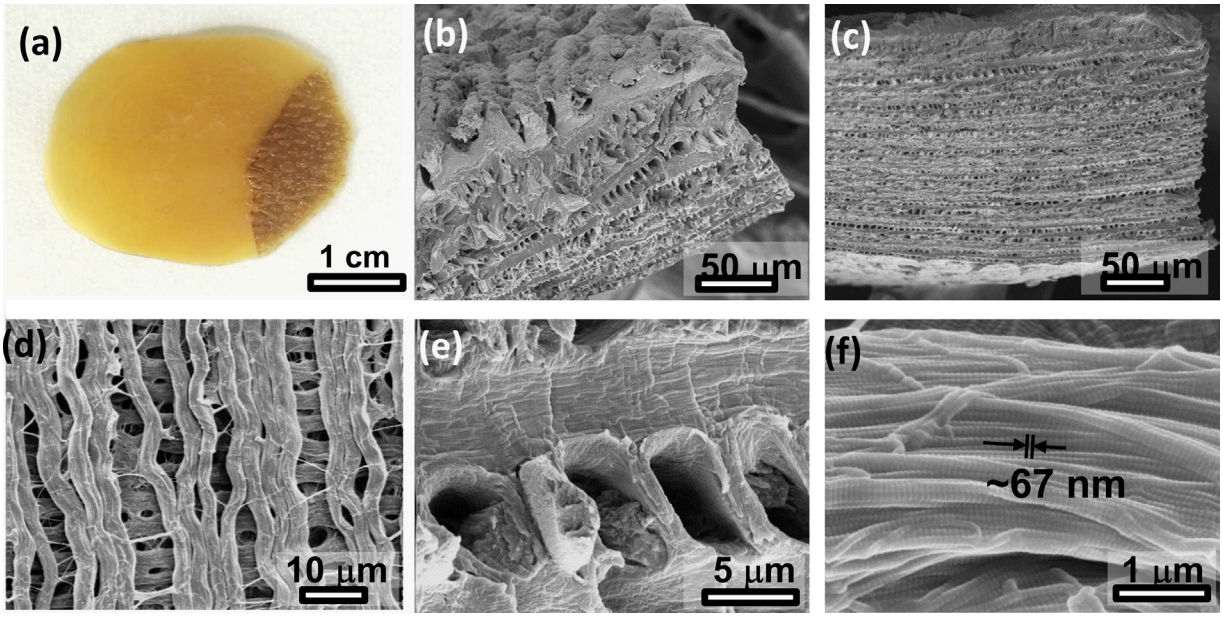

Fig. 24 – Structure of the coelacanth scale. (a) Macroscopic view of coelacanth scale. (b) Perspective view of scale showing external mineralized layer and lamellae. (c) Cross-sectional view of coelacanth scales. (d) Top view of peeled surface showing two adjacent collagen lamellae oriented close to (but not exactly) 90 degrees. (e) Struts between adjacent lamellae forming perpendicular to their plane and connecting them. (f) Collagen fibrils with characteristic d spacing of 67 nm forming the collagen bundle/fiber (from Quan et al. (2015)).

who also pointed out that this configuration provides in-plane isotropy, which is important for resistance to crack propagation. This type of structure is known as "Bouligand-like". In contrast to elasmoid scale of the arapaimas and most teleost fish, the scale of the coelacanth contains struts that connect adjacent lamellae. These are shown in Fig. 24e. The collagen fibers curve at the extremities of the struts. This configuration provides a greater rigidity to the scale by reducing sliding between the lamellae. The confirmation that the fibers are indeed collagen is provided in Fig. 24f, which shows the characteristic banding of ~67 nm.

7. Collagen in bones, teeth, and other tissues

Another biological material which owes its impressive properties to collagen is bone. In a human body, the bone structure (skeleton) supports the entire weight of the body, yet only represents ~20% of the total weight. Bone must possess exceptional mechanical properties in order to fulfill its role. Fig. 25a shows a schematic of bone, and Fig. 25b shows the results of mechanical testing on bone. There is an asymmetry with the longitudinal compressive strength (200 MPa) being higher than the tensile strength (150 MPa). The mechanical response shown in Fig. 25b is due to the hierarchical structure shown in Fig. 25c, which contains blood vessels, osteons, concentric and interstitial lamellae and more. The bone is composed of the mineral and organic matrix, of which 90% is collagen. The collagen and mineral govern the mechanical properties and functional integrity of this tissue (Knott and Bailey, 1998). The mineral acts as a reinforcement in the collagen fibrillar network to provide specialized mechanical properties. Nudelman et al. (2010) investigated the mineralization of the collagen fibrils and claimed that by controlling the mineral nucleation, collagen can direct the mineralization actively. With mineral reinforcement, collagen shows a Young's modulus of 5–10 GPa and yield tensile strain of ~7%, as opposed to non-mineralized collagen with a Young's modulus of ~1 GPa (Buehler, 2007).

Gupta et al. (2006) investigated the roles of the mineral and collagen in bone, in particular the slip of the mineralized collagen fibrils, by studying the relationship between the tissue strain and local strains of mineral and fibrils. The strain ratio of the tissue, collagen fibril and mineral is 12:5:2, meaning that the mineral only takes up a small amount of strain, while the majority of the strain is absorbed by collagen fibrillar and interfibrillar sliding, in addition to other mechanisms.

Launey et al. (2010) summarized the toughening mechanisms of bone which can be greatly attributed to the mineralized collagen fibrils. These mechanisms were classified into intrinsic and extrinsic, following what had been previously defined in synthetic materials by Ritchie (2011). The intrinsic toughening mechanisms are typically ahead of the crack, while the extrinsic mechanisms operate in the wake region. The schematic drawing in Fig. 26a illustrates the intrinsic and extrinsic toughening mechanisms of bone. The toughness of the bone is attributed to both extrinsic mechanisms including crack deflection and twist, uncracked-ligment bridging, collagen fibril bridging and some microcracks in the structure, and intrinsic mechanisms which are induced by the plastic deformation in the microstructure, such as molecular uncoiling and intermolecular sliding of molecules, microcracking, fibrillar sliding, and the breaking of sacrificial bonds together with crack bridging by collagen fibrils. Fig. 26b shows the toughness of human cortical bone as it evolves with crack size. It increase with size demonstrates that the extrinsic mechanisms are operating, rendering propagation more difficult as the crack grows. There are clear differences with

Please cite this article as: Sherman, V.R., et al., The materials science of collagen. Journal of the Mechanical Behavior of Biomedical Materials (2015), http://dx.doi.org/10.1016/j.jmbbm.2015.05.023

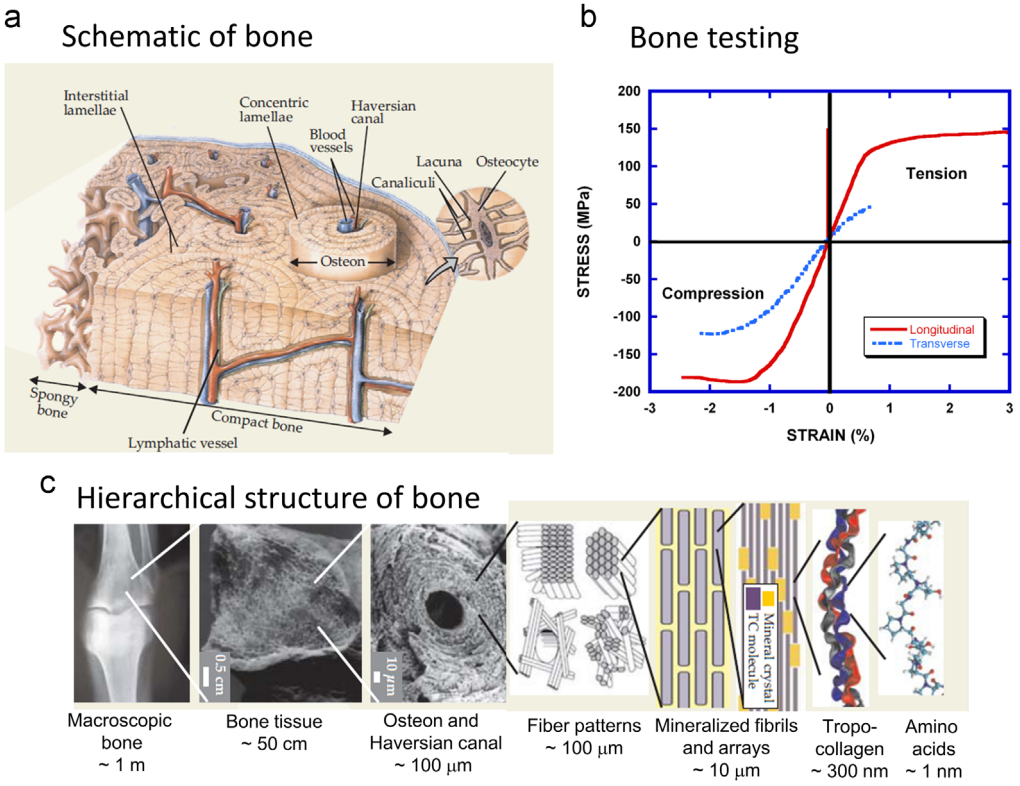

Fig. 25 – The hierarchical structure of bone. (a) A schematic shows both spongy and compact bone, and the arrangement of the osteons, lamella, and Haversian canals within. (b) Tensile and compressive stress–strain curves for cortical bone (Lucas et al., 1999). (c) The hierarchical structure of bone from the macroscopic level down to the amino acid level (Ritchie et al., 2009).

orientation, the longitudinal toughness being significantly lower than the transverse one. Long bones cracks preferentially along their axes because of the anisotropy in the organization of the microstructure. The response of elk antler is given in the same plot, for comparison. The extrinsic mechanisms operate as effectively for antler as for bone. The transverse toughness of bone increases from 1 to >10 MPa $m^{1/2}$ as the crack grows from $\sim$0.01 to $\sim$0.6 mm. This toughening is extremely important for preventing fractures but unfortunately decreases with age.

As bones age the quality of the collagen decreases, greatly affecting the mechanical properties. This degradation of the mechanical integrity of the collagen network in bone due to aging was demonstrated by Zioupos (2001, Zioupos et al., 1999) and quantified by Nalla et al. (2006). In the case of disease such as osteoporosis, this was demonstrated by Wang et al. (2002) and Currey (2003). As aging occurs, the bridges weaken and hence toughness of the bone decreases (Ritchie, 2010).

8. Designer collagen

Thus far, collagen molecules have not been synthesized. However, collagen fibrils have been produced through a process of dissolution of natural collagen, followed by processing and assembly. This process may best be described as guided self-assembly. Collagen structures may be manufactured in a laboratory environment, and have potential uses for the replacement of ligaments and skin, and building scaffolds. Collagen based constructs with tailored properties have great value for clinical uses. A variety of methods has been developed to design and produce collagen structures. There are methodologies to dissolve collagen and processes to create collagen filaments, strands, ribbons, films, sheets, and pre-shaped implants. More recently, a goal has been to synthesize fibers most like those produced by the fibroblasts in the body.

There are currently nearly 1000 readily searchable patents which mention collagen. Early patents, starting in the 1950s, discuss collagen filaments, sheets, etc. In the 1960s, the focus was placed on methods for solubilizing collagen fibers for usage. Around the 1970s, methods were developed to use collagen as prosthetics and implants. The collagen structures which are produced continue to become more advanced; in 1989, Silver attempted to precisely control the geometry and structure of a collagen matrix, filing a patent on synthetic collagen orthopedic structures (Silver and Kato, 1992). Since the 1950s, research on biodegradable synthetic collagen structures has continued with great success, as methods have been refined. Synthetic fibrils and scaffolds are now produced with properties approaching what is found in the body (Gentleman et al., 2003; Roeder et al., 2002; Pins et al., 1997).

9. Conclusions

Collagen is a protein of crucial importance. Starting from the molecular level, a complex and refined hierarchical structure leads to a plethora of natural and synthesized materials with

Please cite this article as: Sherman, V.R., et al., The materials science of collagen. Journal of the Mechanical Behavior of Biomedical Materials (2015), http://dx.doi.org/10.1016/j.jmbbm.2015.05.023

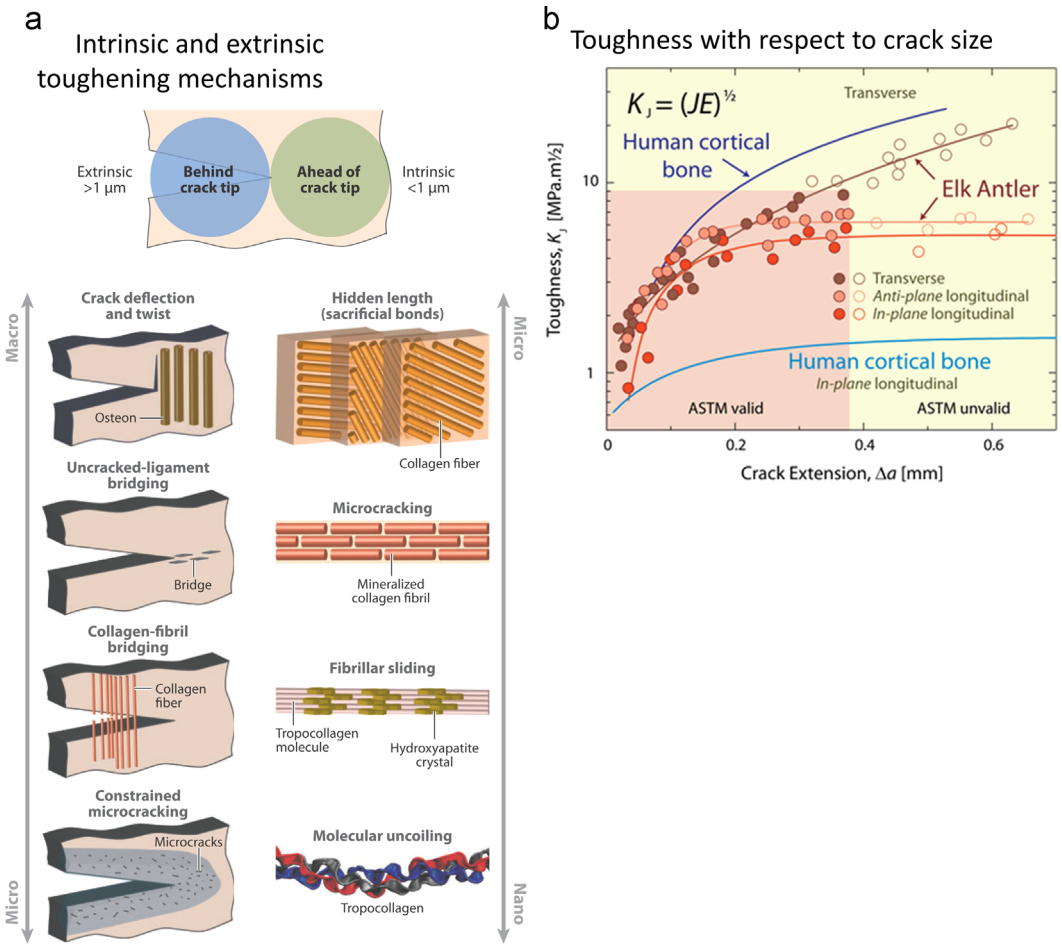

Fig. 26 – Toughening mechanisms of bone. (a) Extrinsic mechanisms occur behind the crack tip, while intrinsic mechanisms occur ahead of the crack tip. Launey et al. (2010) (b) Crack–resistance curves showing resistance to fracture in as a function of crack extension, Δa, for hydrated antler and human compact bone in different orientations Launey et al. (2010).

a broad range of mechanical properties. Through advanced characterization methods these structures are becoming better understood, clarifying the essential connection between structure and function. Nevertheless, in spite of many years of research, there are still many aspects of this material which are not fully understood and instances where conflicting views have not been resolved. This reflects the immense opportunities for research.

There are areas where research continues to shed new light and full understanding is still incomplete. Among these are: a) constitutive equations based on observation which fully incorporate anisotropy, b) full analytical incorporation of viscoelastic response into the constitutive description, c) complete understanding of the contributions and collagen and mineral components of biological composites and d) improved synthesis methods of collagen to reproduce biological patterns.

In the future, a more complete understanding of the many aspects of collagen may lead to improved disease treatment in the biological realm and the creation of synthetic materials with tailored properties in ways which were not previously possible. Understanding of existing and yet to be studied collagen-based materials will reveal instances of convergent evolution, which will provide inspiration for synthetic materials. The increasing knowledge of the atomistic structure of collagen enables scientists to study and understand their performance, and how minor changes can have profound effects on their function. Challenges arise in modeling due to difficulties in testing and evaluating nanoscale sized features, and due to computational limits of atomistic simulations generated by the large number of atoms in collagen, but improved instrumentation and computational abilities continue to expand the realm of possibilities. The role that materials science is playing is pivotal, because the methodologies of characterizing, testing, and modeling of collagen structures are significantly enhancing our understanding. In this review we presented the foundations of the materials science approach and then focused on a few cases, mostly related to our own research. These examples illustrate how this vast volume of information on collagen is undergoing rapid expansion and how this contributes to a quantitative understanding of the structural and functional response of collagen-based materials.

Acknowledgments

This study was supported by the University of California Lab Research Program, Grant no. 09-LR-06-118456-MEYM. We thank Dr. Y.-Z. Tang for the calculated stress–strain response

Please cite this article as: Sherman, V.R., et al., The materials science of collagen. Journal of the Mechanical Behavior of Biomedical Materials (2015), http://dx.doi.org/10.1016/j.jmbbm.2015.05.023

of the wire. We thank Profs. J. McKittrick and R. O. Ritchie for discussions. Mason Mackey kindly assisted us in the TEM sample preparation, and Maria I. Lopez and Shiteng Zhao helped by operating the TEM. We also gratefully acknowledge partial financial support from a Multi-University Research Initiative through the Air Force Office of Scientific Research (AFOSR-FA9550-15-1-0009).

Appendix

The derivatives of the strain energy (or Helmholtz free energy per unit volume, in the case where the volume is constant) with respect to stretch is equal to, by definition:

$$\sigma_1 = \frac{\partial W}{\partial \lambda_1} \tag{A1}$$

$$\sigma_2 = \frac{\partial W}{\partial \lambda_2} \tag{A2}$$

$$\sigma_3 = \frac{\partial W}{\partial \lambda_3} \tag{A3}$$

Where $\sigma_1, \sigma_2, \sigma_3$ are the principal stresses and $\lambda_1, \lambda_2, \lambda_3$ are the principal stretches. Here, assuming constancy of volume:

$$\lambda_1\lambda_2\lambda_3 = 1 \tag{A4}$$

If λ_1 and $\lambda_2$are considered independent variables (for a sheet being stretched in plane OX_1X_2):

$$\lambda_3 = \frac{1}{\lambda_1\lambda_2} \tag{A5}$$

$$\partial\lambda_3 = \frac{1}{\lambda_1^2\lambda_2}\partial\lambda_1 + \frac{1}{\lambda_2^2\lambda_1}\partial\lambda_2 \tag{A6}$$

Inserting the constancy of volume and equilibrium condition:

$$\delta W = \sigma_1\lambda_2\lambda_3\delta\lambda_1 + \sigma_2\lambda_3\lambda_1\delta\lambda_2 + \sigma_3\lambda_1\lambda_2\delta\lambda_3 \tag{A7}$$

we obtain:

$$\delta W = \left(\frac{\sigma_1-\sigma_3}{\lambda_1}\right)\delta\lambda_1 + \left(\frac{\sigma_1-\sigma_3}{\lambda_2}\right)\delta\lambda_2 \tag{A8}$$

When stretches change by $\partial\lambda_1$and $\partial\lambda_2$, the Helmholtz free energy changes by:

$$\delta W = \frac{\partial W(\lambda_1,\lambda_2)}{\partial\lambda_1}\delta\lambda_1 + \frac{\partial W(\lambda_1,\lambda_2)}{\partial\lambda_2}\delta\lambda_2 \tag{A9}$$

Comparing the two previous equations, we obtain:

$$\sigma_1 - \sigma_3 = \lambda_1\frac{\partial W(\lambda_1,\lambda_2)}{\partial\lambda_1} \tag{A10}$$

$$\sigma_2 - \sigma_3 = \lambda_2\frac{\partial W(\lambda_1,\lambda_2)}{\partial\lambda_2} \tag{A11}$$

Eq. (A10) is Eq. (2) in the text. It enables obtaining the difference in stresses from the strain energy derivative with respect to the stretch ratios. This is the foundation of hyperelastic macroscopic models based on strain energy.

REFERENCES

Bächinger, H.P., et al., 2010. Collagen formation and structure. In: Mander, L.N., Liu, H.-W., Vederas, J.C. (Eds.), Comprehensive Natural Products II Chemistry and Biology. Elsevier, Amsterdam, New York, Paris, pp. 469–528.

Benedict, J.V., Walker, L.B., Harris, E.H., 1968. Stress–strain characteristics and tensile strength of unembalmed human tendon. J. Biomech. 1 (1), 53–63.

Beskos, D.E., Jenkins, J.T., 1975. Mechanical model for mammalian tendon. J. Appl. Mech. 42 (4), 755–758.

Bhole, A.P., et al., 2009. Mechanical strain enhances survivability of collagen micronetworks in the presence of collagenase: implications for load-bearing matrix growth and stability. Philos. Trans. R. Soc. A 367 (1902), 3339–3362.

Birk, D.E., Trelstad, R.L., 1986. Extracellular compartments in tendon morphogenesis – collagen fibril, bundle, and macroaggregate formation. J. Cell Biol. 103 (1), 231–240.

Blatz, P.J., Mae Chu, B., Wayland, H., 1969. On the mechanical behavior of elastic animal tissue. Trans. Soc. Rheol. 13 (1), 83–102.

Brodsky, B., Persikov, A.V., 2005. Molecular structure of the collagen triple helix. Fibrous Proteins: Coiled-Coils Collagen and Elastom. 70, 301–339.

Bryant, M.R., et al., 1994. Corneal tensile-strength in fully healed radial keratotomy wounds. Investig. Ophthalmol. Vis. Sci. 35 (7), 3022–3031.

Buehler, M.J., 2006. Atomistic and continuum modeling of mechanical properties of collagen: elasticity, fracture, and self-assembly. J. Mater. Res. 21 (8), 1947–1961.

Buehler, M.J., 2006. Nature designs tough collagen: explaining the nanostructure of collagen fibrils. Proc. Natl. Acad. Sci. USA 103 (33), 12285–12290.

Buehler, M.J., 2007. Molecular nanomechanics of nascent bone: fibrillar toughening by mineralization. Nanotechnology 18 (29), 1–9.

Buehler, M.J., 2008. Nanomechanics of collagen fibrils under varying cross-link densities: atomistic and continuum studies. J. Mech. Behav. Biomed. Mater. 1 (1), 59–67.

Bustamante, C., et al., 1994. Entropic Elasticity of λ-phage DNA. Science 265 (5178), 1599–1600.

Canty, E.G., et al., 2004. Coalignment of plasma membrane channels and protrusions (fibripositors) specifies the parallelism of tendon. J. Cell Biol. 165 (4), 553–563.

Chen, P.Y., McKittrick, J., Meyers, M.A., 2012. Biological materials: functional adaptations and bioinspired designs, Prog. Mater. Sci. 57 (8), 1492–1704.

Cho, G.Y., Wu, Y.T., Ackerman, J.L., 2003. Detection of hydroxyl ions in bone mineral by solid-state NMR spectroscopy. Science 300 (5622), 1123–1127.

Cintron, C., Covington, H., Kublin, C.L., 1983. Morphogenesis of rabbit corneal stroma. Investig. Ophthalmol. Vis. Sci. 24 (5), 543–556.

Comninou, M., Yannas, I.V., 1976. Dependence of stress–strain nonlinearity of connective tissues on geometry of collagen-fibers. J. Biomech. 9 (7), 427–433.

Currey, J.D., 2003. Role of collagen and other organics in the mechanical properties of bone. Osteoporos. Int. 14 (Suppl. 5), S29–S36.

Cusack, S., Miller, A., 1979. Determination of the elastic-constants of collagen by brillouin light-scattering. J. Mol. Biol. 135 (1), 39–51.

Dale, W.C., et al., 1972. On the ultrastructure of mammalian tendon. Experientia 28 (11), 1293–1295.

Dastjerdi, K.A., Barthelat, F., 2014. Teleost fish scales amongst the toughest collagenous materials. J. Mech. Behav. Biomed. Mater., in press [pii: S1751-6161(14)00309-9].

Diamant, J., et al., 1972. Collagen – ultrastructure and its relation to mechanical properties as a function of aging. Proc. R. Soc. Ser. B 180 (1060), 293–315.

Doehring, T.C., Carew, E.O., Vesely, I., 2004. The effect of strain rate on the viscoelastic response of aortic valve tissue: a direct-fit approach. Ann. Biomed. Eng. 32 (2), 223–232.

Eppell, S.J., et al., 2006. Nano measurements with micro-devices: mechanical properties of hydrated collagen fibrils. J. R. Soc. Interface 3 (6), 117–121.

Eyre, D.R., Wu, J.-J., 2005. Collagen cross-links. Topics in Current Chemistry, vol. 247. Springer-Verlag, Berlin, 207–229.

Franke, O., et al., 2011. Dynamic nanoindentation of articular porcine cartilage. Mater. Sci. Eng. C 31 (4), 789–795.

Franzke, C.W., Bruckner, P., Bruckner-Tuderman, L., 2005. Collagenous transmembrane proteins: recent insights into biology and pathology. J. Biol. Chem. 280 (6), 4005–4008.

Fratzl, P., et al., 2004. Structure and mechanical quality of the collagen-mineral nano-composite in bone. J. Mater. Chem. 14, 2115–2123.

Fung, Y.C., 1993. In: Biomechanics : Mechanical Properties of Living Tissues 2nd ed. Springer-Verlag, New York.

Fung, Y.C., 1981. Biomechanics: Mechanical Properties of Living Tissues. Springer-Verlag, New York433.

Fung, Y.C., 1967. Elasticity of soft tissues in simple elongation. Am. J. Physiol. 213 (6), 1532–1544.

Gautieri, A., Buehler, M.J., Redaelli, A., 2009. Deformation rate controls elasticity and unfolding pathway of single tropocollagen molecules. J. Mech. Behav. Biomed. Mater. 2 (2), 130–137.

Gautieri, A., et al., 2010. Coarse-grained model of collagen molecules using an extended MARTINI force field. J. Chem. Theory Comput. 6 (4), 1210–1218.

Gautieri, A., et al., 2011. Hierarchical structure and nanomechanics of collagen microfibrils from the atomistic scale up. Nano Lett. 11 (2), 757–766.

Gautieri, A., et al., 2012. Hydration and distance dependence of intermolecular shearing between collagen molecules in a model microfibril. J. Biomech. 45 (12), 2079–2083.

Gelman, R.A., Williams, B.R., Piez, K.A., 1979. Collagen fibril formation – evidence for a multistep process. J. Biol. Chem. 254 (1), 180–186.

Gelse, K., Poschl, E., Aigner, T., 2003. Collagens – structure, function, and biosynthesis. Adv. Drug Deliv. Rev. 55 (12), 1531–1546.

Gentleman, E., et al., 2003. Mechanical characterization of collagen fibers and scaffolds for tissue engineering. Biomaterials 24 (21), 3805–3813.

Giraud, M.M., et al., 1978. The fibrous structure of coelacanth scales: a twisted 'plywood'. Tissue Cell 10 (4), 671–686.

Gupta, H.S., et al., 2004. Synchrotron diffraction study of deformation mechanisms in mineralized tendon. Phys. Rev. Lett. 93 (15), 158101.

Gupta, H.S., et al., 2006a. Mechanical modulation at the lamellar level in osteonal bone. J. Mater. Res. 21 (8), 1913–1921.

Gupta, H.S., et al., 2006b. Cooperative deformation of mineral and collagen in bone at the nanoscale. Proc. Natl. Acad. Sci. USA 103 (47), 17741–17746.

Hansen, K.A., Weiss, J.A., Barton, J.K., 2002. Recruitment of tendon crimp with applied tensile strain. J. Biomech. Eng. 124 (1), 72–77.

Harley, R., et al., 1977. Phonons and the elastic moduli of collagen and muscle. Nature 267 (5608), 285–287.

Haut, R.C., 1986. The influence of specimen length on the tensile failure properties of tendon collagen. J. Biomech. 19 (11), 951–955.

Hay, E.D., Revel, J.P., 1969. Fine structure of the developing avian cornea. Monogr. Dev. Biol. 1, 1–144.

Hofmann, H., et al., 1984. Localization of flexible sites in thread-like molecules from electron-micrographs – comparison of interstitial, basement-membrane and intima collagens. J. Mol. Biol. 172 (3), 325–343.

Hulmes, D.J.S., 2008. Collagen diversity, synthesis and assembly. In: Fratzl, P. (Ed.), Collagen: Structure and Mechanics. Springer, New York, pp. 15–47.

Kadler, K.E., et al., 2007. Collagens at a glance. J. Cell Sci. 120 (12), 1955–1958.

Kastelic, J., Palley, I., Baer, E., 1980. A structural mechanical model for tendon crimping. J. Biomech. 13 (10), 887–893.

Kato, Y.P., et al., 1989. Mechanical-properties of collagen-fibers – a comparison of reconstituted and rat tail tendon fibers. Biomaterials 10 (1), 38–41.

Knott, L., Bailey, A.J., 1998. Collagen cross-links in mineralizing tissues: a review of their chemistry, function, and clinical relevance. Bone 22 (3), 181–187.

Koester, K.J., Ager 3rd, J.W., Ritchie, R.O., 2008. The true toughness of human cortical bone measured with realistically short cracks. Nat. Mater. 7 (8), 672–677.

Landis, W.J., et al., 1996. Structural relations between collagen and mineral in bone as determined by high voltage electron microscopic tomography. Microsc. Res. Tech. 33 (2), 192–202.

Landis, W.J., Hodgens, K.J., 1996. Mineralization of collagen may occur on fibril surfaces: evidence from conventional and high-voltage electron microscopy and three-dimensional imaging. J. Struct. Biol. 117 (1), 24–35.

Lanir, Y., 1978. Structure-strength relations in mammalian tendon. Biophys. J. 24 (2), 541–554.

Lanir, Y., Fung, Y.C., 1974. Two-dimensional mechanical properties of rabbit skin. II. Experimental results. J. Biomech. 7 (2), 171–182.

Launey, M.E., Buehler, M.J., Ritchie, R.O., 2010. On the mechanistic origins of toughness in bone. Annu. Rev. Mater. Res. 40 (1), 25–53.

Launey, M.E., et al., 2010. Mechanistic aspects of the fracture toughness of elk antler bone. Acta Biomater. 6 (4), 1505–1514.

Lees, S., 1979. A model for the distribution of HAP crystallites in bone – an hypothesis. Calcif. Tissue Int. 27 (1), 53–56.

Leighton, M., Kadler, K.E., 2003. Paired basic/furin-like proprotein convertase cleavage of pro-BMP-1 in the trans-Golgi network. J. Biol. Chem. 278 (20), 18478–18484.

Leslie, M., 2006. Making tendons. J. Cell Biol. 172 (2), 167.

Lin, Y.S., et al., 2011. Mechanical properties and the laminate structure of Arapaima gigas scales. J. Mech. Behav. Biomed. Mater. 4 (7), 1145–1156.

Lorenzo, A.C., Caffarena, E.R., 2005. Elastic properties, Young's modulus determination and structural stability of the tropocollagen molecule: a computational study by steered molecular dynamics. J. Biomech. 38 (7), 1527–1533.

Lucas, G.L., Cooke, F.W., Friis, E.A., 1999. In: A Primer on Biomechanics. Springer, New York, 268.

Markenscoff, X., Yannas, I.V., 1979. On the stress–strain relation for skin. J. Biomech. 12 (2), 127–129.

Marrink, S.J., et al., 2007. The MARTINI force field: coarse grained model for biomolecular simulations. Journal of Physical Chemistry B 111 (27), 7812–7824.

Meyers, M.A., Chen, P.-Y., 2014. Biological Materials Science: Biological Materials, Bioinspired Materials, and BiomaterialsCambidge University Press, Cambridge, UK.

Miyazaki, H., Hayashi, K., 1999. Tensile tests of collagen fibers obtained from the rabbit patellar tendon. Biomed. Microdevices 2 (2), 151–157.

Morgan, F.R., 1960. The mechanical properties of collagen fibers: stress–strain curves. J. Soc. Leather Trades Chem. 44, 170–182.

Myllyharju, J., Kivirikko, K.I., 2001. Collagens and collagen-related diseases. Ann. Med. 33 (1), 7–21.

Nalla, R.K., et al., 2006. Role of microstructure in the aging-related deterioration of the toughness of human cortical bone. Mater. Sci. Eng. C: Biomim. Supramol. Syst. 26 (8), 1251–1260.

Nestler, F.H.M., et al., 1983. Flexibility of Collagen Determined from Dilute-Solution Viscoelastic Measurements. Biopolymers 22 (7), 1747–1758.

Please cite this article as: Sherman, V.R., et al., The materials science of collagen. Journal of the Mechanical Behavior of Biomedical Materials (2015), http://dx.doi.org/10.1016/j.jmbbm.2015.05.023

Nudelman, F., et al., 2010. The role of collagen in bone apatite formation in the presence of hydroxyapatite nucleation inhibitors. Nat. Mater. 9 (12), 1004–1009.

Ogden, R.W., 1984. Non-Linear Elastic Deformations, second ed. Ellis Harwood Ltd, Chichester, England, Dover, 1997.

Okuyama, K., et al., 2006. Revision of collagen molecular structure. Biopolymers 84 (2), 181–191.

Olsen, B.R., 1963. Electron microscope studies on collagen. 1. Native collagen fibrils. Z. Zellforsch. Mikrosk. Anat. 59 (2), 184–198.

Orgel, J.P.R.O., et al., 2006. Microfibrillar structure of type I collagen in situ. Proc. Natl. Acad. Sci. USA 103 (24), 9001–9005.

Orgel, J.P.R.O., Antonio, J.D.S., Antipova, O., 2011. Molecular and structural mapping of collagen fibril interactions. Connect. Tissue Res. 52 (1), 2–17.

Orssengo, G.J., Pye, D.C., 1999. Determination of the true intraocular pressure and modulus of elasticity of the human cornea in vivo. Bull. Math. Biol. 61 (3), 551–572.

Pasquinelli, G., 2010. Fibrohistiocytic tumors containing zebra body-like inclusions and fibripositors. Ultrastruct. Pathol. 34 (6), 366–370.

Pasteris, J.D., et al., 2012. Effect of carbonate incorporation on the hydroxyl content of hydroxylapatite. Mineral. Mag. 76 (7), 2741–2759.

Pins, G.D., et al., 1997. Self-assembly of collagen fibers. Influence of fibrillar alignment and decorin on mechanical properties. Biophys. J. 73 (4), 2164–2172.

Pradhan, S., Katti, D., Katti, K., 2011. Steered molecular dynamics study of mechanical response of full length and short collagen molecules. J. Nanomech. Micromech. 1 (3), 104–110.

Puxkandl, R., et al., 2002. Viscoelastic properties of collagen: synchrotron radiation investigations and structural model. Philos. Trans. R. Soc. Lond. Ser. B – Biol. Sci. 357 (1418), 191–197.

Qin, Z., Buehler, M.J., 2011. Flaw tolerance of nuclear intermediate filament lamina under extreme mechanical deformation. ACS Nano 5 (4), 3034–3042.

Qin, Z., Buehler, M.J., 2013. Impact tolerance in mussel thread networks by heterogeneous material distribution. Nat. Commun. 4 (2187), 1–8.

Quan, H., Yang, W., and Meyers, M.A., 2015. The Relationship between Structure and Properties in Coelacanth Scales. Unpublished results.

Rey, C., et al., 1995. Hydroxyl-groups in bone-mineral. Bone 16 (5), 583–586.

Ridge, M.D., Wright, V., 1964. The description of skin stiffness. Biorheology 2, 67–74.

Rigby, B.J., et al., 1959. The mechanical properties of rat tail tendon. J. Gen. Physiol. 43 (2), 265–283.

Ritchie, R.O., 2010. How does human bone resist fracture?. Skelet. Biol. Med. 1192, 72–80.

Ritchie, R.O., 2011. The conflicts between strength and toughness. Nat. Mater. 10 (11), 817–822.

Ritchie, R.O., Buehler, M.J., Hansma, P., 2009. Plasticity and toughness in bone. Phys. Today 62 (6), 41–47.

Roeder, B.A., et al., 2002. Tensile mechanical properties of three-dimensional type I collagen extracellular matrices with varied microstructure. J. Biomech. Eng. 124 (2), 214–222.

Ruberti, J.W., Zieske, J.D., 2008. Prelude to corneal tissue engineering – gaining control of collagen organization. Prog. Retin. Eye Res. 27 (5), 549–577.

Sasaki, N., Odajima, S., 1996. Elongation mechanism of collagen fibrils and force–strain relations of tendon at each level of structural hierarchy. J. Biomech. 29 (9), 1131–1136.

Sasaki, N., Odajima, S., 1996. Stress–strain curve and Young's modulus of a collagen molecule as determined by the X-ray diffraction technique. J. Biomech. 29 (5), 655–658.

Shadwick, R.E., Russell, A.P., Lauff, R.F., 1992. The structure and mechanical design of rhinoceros dermal armor. Philos. Trans. R. Soc. Lond. Ser. B – Biol. Sci. 337 (1282), 419–428.

Shen, Z.L., et al., 2008. Stress–strain experiments on individual collagen fibrils. Biophys. J. 95 (8), 3956–3963.

Sherman, V.R., Tang, Y.Z., and Meyers, M.A., 2015. Unpublished Results.

Silver, F.H. and Kato, Y.P., 1992. Synthetic collagen orthopaedic structures such as grafts, tendons and other structures. Google Patents.

Silver, F.H., Ebrahimi, A., Snowhill, P.B., 2002. Viscoelastic properties of self-assembled type I collagen fibers: molecular basis of elastic and viscous behaviors. Connect. Tissue Res. 43 (4), 569–580.

Silver, F.H., Freeman, J.W., Seehra, G.P., 2003. Collagen self-assembly and the development of tendon mechanical properties. J. Biomech. 36 (10), 1529–1553.

Smith, J.W., 1965. Packing Arrangement of Tropocollagen Molecules. Nature 205 (4969), 356–358.

Smith, J.W., 1968. Molecular Pattern in Native Collagen. Nature 219 (5150), 157–158.

Sun, Y.L., et al., 2002. Direct quantification of the flexibility of type I collagen monomer. Biochem. Biophys. Res. Commun. 295 (2), 382–386.

Svensson, R.B., et al., 2010. Viscoelastic behavior of discrete human collagen fibrils. J. Mech. Behav. Biomed. Mater. 3 (1), 112–115.

Tong, P., Fung, Y.C., 1976. Stress–strain relationship for skin. J. Biomech. 9 (10), 649–657.

Trelstad, R.L., 1982. The bilaterally asymmetrical architecture of the sub-mammalian corneal stroma resembles a cholesteric liquid-crystal. Dev. Biol. 92 (1), 133–134.

Trelstad, R.L., Hayashi, K., Gross, J., 1976. Collagen fibrillogenesis – intermediate aggregates and supra-fibrillar order. Proc. Natl. Acad. Sci. USA 73 (11), 4027–4031.

Valanis, K.C., Landel, R.F., 1967. Strain-energy function of a hyperelastic material in terms of extension ratios. J. Appl. Phys. 38 (7), 2997–3002.

Vanderrest, M., Mayne, R., 1988. Type-Ix collagen proteoglycan from cartilage is covalently cross-linked to Type-Ii collagen. J. Biol. Chem. 263 (4), 1615–1618.

Veronda, D.R., Westmann, R.A., 1970. Mechanical characterization of skin-finite deformations. J. Biomech. 3 (1), 111–122.

Vesentini, S., et al., 2005. Molecular assessment of the elastic properties of collagen-like homotrimer sequences. Biomech. Model. Mechanobiol. 3 (4), 224–234.

Vesentini, S., Redaelli, A., Gautieri, A., 2013. Nanomechanics of collagen microfibrils. Muscles Ligaments Tendons J. 3 (1), 23–34.

Vuorio, E., Decrombrugghe, B., 1990. The Family of Collagen Genes. Annu. Rev. Biochem. 59, 837–872.

Wainwright, S.A., Biggs, WD, Currey, JD, Gosline, JM., 1982. In: Mechanical Design in Organisms. Princeton Univ. Press, Princeton.

Wang, W.M., et al., 2003. Transforming growth factor-beta induces secretion of activated ADAMTS-2 – a procollagen IIIN-proteinase. J. Biol. Chem. 278 (21), 19549–19557.

Wang, X., et al., 2002. Age-related changes in the collagen network and toughness of bone. Bone 31 (1), 1–7.

Wertheim, M.G., 1847. Memoire sur l'eastocote et la cohesion des principaux tissues du corps humain. Ann. Chim. Phys., 385–41421, 385–414.

Wu, J.J., Woods, P.E., Eyre, D.R., 1992. Identification of cross-linking sites in bovine cartilage Type-Ix collagen reveals an antiparallel Type-Ii-Type-Ix molecular relationship and Type-Ix to Type-Ix bonding. J. Biol. Chem. 267 (32), 23007–23014.

Please cite this article as: Sherman, V.R., et al., The materials science of collagen. Journal of the Mechanical Behavior of Biomedical Materials (2015), http://dx.doi.org/10.1016/j.jmbbm.2015.05.023

Yang, W., et al., 2013a. Natural flexible dermal armor. Adv. Mater. 25 (1), 31–48.

Yang, W., et al., 2013b. Structure and fracture resistance of alligator gar (Atractosteus spatula) armored fish scales. Acta Biomater. 9 (4), 5876–5889.

Yang, W., et al., 2014. Protective role of Arapaima gigas fish scales: structure and mechanical behavior. Acta Biomater. 10 (8), 3599–3614.

Yang, W., et al., 2015. On the tear resistance of skin, Nat. Commun. 6, 1-10.

Yannas, I.V., Huang, C., 1972. Fracture of tendon collagen. J. Polym. Sci. Part A – 2: Polym. Phys. 10 (4), 577–584.

Zhu, D.J., et al., 2012. Structure and mechanical performance of a "Modern" fish scale. Adv. Eng. Mater. 14 (4), B185–B194.

Zioupos, P., 2001. Ageing human bone: factors affecting its biomechanical properties and the role of collagen. J. Biomater. Appl. 15 (3), 187–229.

Zioupos, P., Currey, J.D., Hamer, A.J., 1999. The role of collagen in the declining mechanical properties of aging human cortical bone. J. Biomed. Mater. Res. 45 (2), 108–116.

van der Rijt, J.A.J., et al., 2006. Micromechanical testing of individual collagen fibrils. Macromol. Biosci. 6 (9), 697–702.

Please cite this article as: Sherman, V.R., et al., The materials science of collagen. Journal of the Mechanical Behavior of Biomedical Materials (2015), http://dx.doi.org/10.1016/j.jmbbm.2015.05.023